

Restoring the Point-and-Charge Gradient Expansion for the Strong Interaction Density Functionals

Lucian A. Constantin,¹ F. Naeem,^{2,3} E. Fabiano,^{1,2} F. Sarcinella,^{1,2} and Fabio Della Sala^{1,2}

¹*Institute for Microelectronics and Microsystems (CNR-IMM),
Via Monteroni, Campus Unisalento, 73100 Lecce, Italy*

²*Center for Biomolecular Nanotechnologies, Istituto Italiano di Tecnologia, Via Barsanti 14, 73010 Arnesano (LE), Italy*

³*Dipartimento di Matematica e Fisica, Università del Salento, Via per Monteroni, 73100 Lecce, Italy*
(Dated: March 9, 2026)

The strong-interaction functionals $W_\infty[n]$ and $W'_\infty[n]$ play an important role in the adiabatic-connection method of Density Functional Theory. The strictly-correlated electron approach can be used to exactly compute these functionals, yet calculations are computationally very expensive even for small electronic systems, and thus semilocal approximations have been proposed. In this work we develop a meta-generalized gradient approximation (meta-GGA) model for the strong-interaction functionals, enhanced point-and-charge (ePC), constructed from exact constraints. In particular, the ePC restores the second-order gradient expansion of the PC model, that is relevant for the equilibrium properties of Wigner crystals, and ensures the non-negativity of $W'_\infty[n]$. We assess the ePC model for atoms and various model systems: Hooke's atoms, two-electron exponential densities, *s*- and *p*-hydrogenic shells, quasi-two-dimensional infinite barrier model, perturbed uniform electron gas and H_2 dissociation. We prove a good overall accuracy of the ePC model, that achieves a broader applicability than any previous semilocal models.

PACS numbers: 71.10.Ca, 71.15.Mb, 71.45.Gm

I. INTRODUCTION

The Kohn-Sham (KS) Density Functional Theory (DFT) [1, 2] is the most used theoretical method in electronic structure calculations [3–7]. The KSDFPT success is based on its simplicity and accuracy, using only the electronic density $n(\mathbf{r})$ as the basic variable which determines all the ground-state properties of the electronic system [8, 9].

The accuracy of the KSDFPT is directly dependent on the approximation used for the exchange-correlation (XC) energy functional [10]. In the KSDFPT adiabatic connection (AC) method [11–17], the XC energy functional $E_{xc}[n]$ is defined as

$$E_{xc}[n] = \int_0^1 d\alpha W_{xc,\alpha}[n], \quad (1)$$

$$W_{xc,\alpha}[n] = \langle \Psi_n^{min,\alpha} | \hat{V}_{ee} | \Psi_n^{min,\alpha} \rangle - U[n], \quad (2)$$

where $U[n] = (1/2) \int d\mathbf{r} \int d\mathbf{r}' n(\mathbf{r})n(\mathbf{r}')/|\mathbf{r} - \mathbf{r}'|$ is the Hartree energy, \hat{V}_{ee} is the Coulomb repulsion operator, and $\Psi_n^{min,\alpha}$ is the antisymmetric wave function that yields the density $n(\mathbf{r})$ and minimizes the expectation value $\langle \hat{T} + \alpha \hat{V}_{ee} \rangle$. Thus, $\Psi_n^{min,\alpha}$ is the ground-state wave-function of an N -electron system with the Hamiltonian [18–21]

$$\begin{aligned} \hat{H}_\alpha[n] &= \hat{T} + \alpha \hat{V}_{ee} + \hat{V}_{ext}^\alpha[n], \\ \hat{V}_{ext}^\alpha[n] &= \sum_{i=1}^N v_{ext}^\alpha([n], \mathbf{r}_i), \end{aligned} \quad (3)$$

where \hat{V}_{ext}^α is the external potential that ensures $\hat{H}_\alpha[n]$ has the same (v -representable) density $n(\mathbf{r})$ for any α .

Here $\alpha \geq 0$ is the coupling constant, also known as the interaction strength.

The AC integrand $W_{xc,\alpha}[n]$ is exactly known in the weak- ($\alpha \rightarrow 0$) and strong- ($\alpha \rightarrow \infty$) interaction limits [22–25]:

$$W_{xc,\alpha \rightarrow 0}[n] = W_0[n] + \sum_{m=2}^{\infty} m E_c^{GLm} \alpha^{m-1}, \quad (4)$$

$$W_{xc,\alpha \rightarrow \infty}[n] = W_\infty[n] + W'_\infty[n] \alpha^{-1/2} + W_\infty^{(2)}[n] \alpha^{-3/2} + \dots, \quad (5)$$

Here, $W_0[n] = E_x^{EXX}[n]$ is the exact DFT exchange functional and E_c^{GLm} is the m -th term of the Görling-Levy (GL) perturbation theory [23, 26, 27]. In the strong-interaction limit, the strictly correlated electron (SCE) approach [28–30] becomes exact, and the square of the SCE wave function for a N -electron system is [18]

$$\begin{aligned} |\Psi_{SCE}(\mathbf{r}_1, \dots, \mathbf{r}_N)|^2 &= \frac{1}{N!} \sum_P \int d\mathbf{r} \frac{n(\mathbf{r})}{N} \delta(\mathbf{r}_1 - f_{P(1)}(\mathbf{r})) \\ &\times \delta(\mathbf{r}_2 - f_{P(2)}(\mathbf{r})) \dots \delta(\mathbf{r}_N - f_{P(N)}(\mathbf{r})), \end{aligned} \quad (6)$$

where f_1, \dots, f_N are comotion functions (with $f_i(\mathbf{r}) = \mathbf{r}$), and P is a permutation of $1, \dots, N$. In the SCE limit, the electrons are well separated from each other, such that the effect on the total energy of the spin state is usually neglected [18–21], being of order $\mathcal{O}(e^{-\alpha^{1/4}})$ [18].

We recall that the set of comotion functions $\{f_i(\mathbf{r})\}$ represents the electron configurations that yield the global (and degenerate) minimum of the asymptotic

potential-energy function

$$E_{pot}([n], \{\mathbf{r}_i\}) = \lim_{\alpha \rightarrow \infty} \frac{\hat{H}_\alpha[n]}{\alpha} = \hat{V}_{ee} + \sum_{i=1}^N v_{SCE}([n], \mathbf{r}_i),$$

$$v_{SCE}([n], \mathbf{r}_i) = \lim_{\alpha \rightarrow \infty} \frac{v_{ext}^\alpha([n], \mathbf{r}_i)}{\alpha}, \quad (7)$$

such that in the SCE limit, the potential energy function $E_{pot}([n], \{f_i(\mathbf{r})\})$ becomes

$$E_{SCE} = W_\infty[n] + U[n] + \sum_{i=1}^N v_{SCE}([n], f_i(\mathbf{r})). \quad (8)$$

For large, but finite $\alpha \gg 1$, the electrons execute small zero-point oscillations around the SCE configuration $\{f_i(\mathbf{s})\}$, such that [18, 19]

$$E_{pot}([n], \{\mathbf{r}_i\}) = E_{SCE} + \frac{1}{2} \sum_{\mu, \nu=1}^{3N} \frac{\partial^2 E_{pot}}{\partial r_\mu \partial r_\nu} \Big|_{\{\mathbf{r}_i\}=\{f_i(\mathbf{s})\}} \times (r_\mu - f_\mu(\mathbf{s}))(r_\nu - f_\nu(\mathbf{s})) + \dots \quad (9)$$

Thus, the strong-interaction functionals in the SCE approach are [18]

$$W_\infty[n] = \int d\mathbf{r} \sum_{i=1}^{N-1} \sum_{j=i+1}^N \frac{n(\mathbf{r})}{N|f_i(\mathbf{r}) - f_j(\mathbf{r})|} - U[n] \quad (10)$$

$$W'_\infty[n] = \frac{1}{4N} \int d\mathbf{r} n(\mathbf{r}) \sum_{\mu=4}^{3N} \omega_\mu(\mathbf{r}) > 0, \quad (11)$$

where $\omega_\mu(\mathbf{r})$ are the frequencies of the local normal modes around the degenerate SCE minimum (i.e. the eigenvalues of the Hessian of the total energy, see Eq. (9)).

The Adiabatic Connection Integrand Interpolation (ACII) XC functionals represent approximations of $W_{xc,\alpha}[n]$, usually constructed from interpolating between the weak- and strong-interaction limits [18, 20–22, 25, 31–54]. Thus, the ACII XC functionals are nonlinear functions of several functionals:

$$E_{xc}^{ACII}[n] = \mathcal{F}(W_0[n], E_c^{GL2}[n], W_\infty[n], W'_\infty[n]), \quad (12)$$

where only the first two terms of the weak- and strong-interaction series (see Eq. (5)) are considered.

Because the SCE approach is computationally very expensive, the ACII XC functionals use semilocal approximations for $W_\infty[n]$ and $W'_\infty[n]$. Here we mention the point-charge-plus-continuum (PC) model [20, 21], its revision revPC [18], the modified PC (mPC) [47] and the harmonium PC (hPC) [50].

The exact PC model has the following GE2 expressions [20, 21]

$$W_\infty^{PC-GE2}[n] = \int d\mathbf{r} A n^{4/3}(\mathbf{r}) F^{PC-GE2}(s), \quad (13)$$

$$W'_\infty^{PC-GE2}[n] = \int d\mathbf{r} C n^{3/2}(\mathbf{r}) F'^{PC-GE2}(s), \quad (14)$$

$$F^{PC-GE2}(s) = 1 - \mu_\infty s^2, \quad (15)$$

$$F'^{PC-GE2}(s) = 1 + \mu'_\infty s^2, \quad (16)$$

where $\mu_\infty = 0.14$ and $\mu'_\infty = 0.491$. Here $A = -1.451$ and $C = 1.535$, while $s = |\nabla n|/[2(3\pi^2)^{1/3}n^{4/3}]$ is the reduced gradient of the density. Note that the exact value $\mu'_\infty = 0.491$ was not considered in any previous PC model; in place of it, negative values (usually $\mu'_\infty = -0.7222$) were used [18, 20, 21, 50], which have been obtained from considerations of atomic/spherical systems [18, 20, 21].

The coupling-constant integrand can be also found from any given XC functional, using the relation [20, 21, 23]

$$W_{xc,\alpha}^{app}[n_\uparrow, n_\downarrow] = \frac{d}{d\alpha} \left(\alpha^2 E_{xc}^{app}[n_{\uparrow,1/\alpha}, n_{\downarrow,1/\alpha}] \right), \quad (17)$$

where $n_{\sigma,1/\alpha} = (1/\alpha^3)n_\sigma(\mathbf{r}/\alpha)$ is the uniformly scaled spin-density. Taking the low-density limit $\alpha \rightarrow \infty$ in Eq. (17), one can extract the $W_\infty^{app}[n_\uparrow, n_\downarrow]$ and $W'_\infty^{app}[n_\uparrow, n_\downarrow]$. Thus, commonly used approximations are the local spin density (LSD) $W_\infty^{LSD}[n_\uparrow, n_\downarrow]$ and $W'_\infty^{LSD}[n_\uparrow, n_\downarrow]$, the Perdew-Burke-Ernzerhof (PBE) [55] generalized gradient approximation (GGA) $W_\infty^{GGA}[n_\uparrow, n_\downarrow]$ and $W'_\infty^{GGA}[n_\uparrow, n_\downarrow]$ and the meta-GGA models $W_\infty^{MGGA}[n_\uparrow, n_\downarrow]$ and $W'_\infty^{MGGA}[n_\uparrow, n_\downarrow]$ [20, 21, 56]. These model approximations for $W_\infty[n]$ and $W'_\infty[n]$ have been tested for various systems [18, 20, 21, 47, 50, 53].

The construction of accurate $W_\infty[n]$ and $W'_\infty[n]$ is of interest not only for the ACII functionals, but also for the DFT development in the low-density regime, e.g. by implying an inverse engineering technique from Eq. (17). In fact, the low-density limit is rich on various phenomena, such as the uniform electron gas (UEG) first-order phase transition from paramagnetic to body-centered cubic crystal at bulk parameter $r_s = 86.6(7)$ [57], the UEG soft plasmon mode [58, 59], or the classical asymptotic behavior of XC potential far from metal surfaces in the vacuum [60]. Finally, we recall that the second-order gradient expansion (GE2) coefficient of the correlation energy is known only in the high-density limit [61], and at the metallic densities (where $2 \leq r_s \leq 6$) [62], but not in the low-density regime where it was approximated from the LSD linear response [63]. In this sense, the gradient expansion of the PC model can be of high interest.

In this work, we construct a meta-GGA model for the strong-interaction functionals $W_\infty[n]$ and $W'_\infty[n]$, named enhanced PC (ePC), that restores the original GE2 of the PC model, and solves several shortcomings of the existing models. In particular, previous models do not guarantee that $W_\infty[n] < 0$ and $W'_\infty[n] > 0$, under all density conditions.

There are not many available benchmark SCE references for $W_\infty[n]$ and $W'_\infty[n]$. In this respect, we report several SCE calculations for two-electron systems and an accurate estimation for quasi-two-dimensional infinite barrier model that may help to judge on the accuracy of the models. Nevertheless, the meta-GGA models for the strong-interaction limit can be further improved

considering additional non-local ingredients, such as the Yukawa potential [64].

The paper is organized as follows: In Sec. II, we present and explain the construction of the ePC model. In Section III, we report the results for atoms and various model systems: Hooke's atoms, two-electron model densities, s - and p -hydrogenic shells, quasi-two-dimensional infinite barrier model, perturbed uniform electron gas and H_2 dissociation; in Sec. IV we present molecular systems, considering for atomization energies and ionization potentials. Finally, in Sec. V, we summarize our conclusions, and in Sec. VI we provide the computational details.

II. THEORY

A. The ePC model for W_∞ :

A meta-GGA expression for W_∞ can be written as:

$$W_\infty^{ePC}[n] = \int d\mathbf{r} A n(\mathbf{r})^{4/3} F^{ePC}(s(\mathbf{r}), z(\mathbf{r})), \quad (18)$$

where $A = -1.451$ and $z = \tau^W/\tau$ is the well-known meta-GGA ingredient [56, 65], with $\tau = \sum_{i=1}^N |\nabla\phi_i|^2/2$ and $\tau^W = |\nabla n|^2/(8n)$ being the positive-defined KS kinetic energy density and the von Weizsäcker kinetic energy density, respectively. (Here ϕ_i is the i -th occupied KS orbital). We recall that z is always bounded between 0 and 1, $z = 1$ for the ground-state of any one- and two-electron (closed-shell) systems, while for a slowly varying density regime, $z \approx (5s^2/3)/(1 + (5s^2/3)) \rightarrow 0$ [56, 65]. Note that Eq. (18) is correctly independent of the spin polarization, see the discussion after Eq. (6).

For $F^{ePC}(s, z)$ we propose the form

$$F^{ePC}(s, z) = F_0(s) + (zF_1(s) - F_0(s))z^p, \quad (19)$$

$$F_1(s) = a_1 + \frac{a_2}{1 + a_3 s^8}, \quad (20)$$

$$F_0(s) = 1 - \kappa + \frac{\kappa}{1 + \frac{\mu_\infty s^2}{\kappa} + \frac{\mu_\infty^2 s^4}{\kappa^2}}, \quad (21)$$

where $F_1(s)$ is the value of F^{ePC} when $z = 1$ (i.e. for one and two-electron systems) and $F_0(s)$ is the value of F^{ePC} when $z = 0$ (e.g. in the UEG), and p is a parameter to be fixed.

Note that $F_0(s)$ and $F_1(s)$ are simple GGA expressions: $F_0(s)$ is constructed to be accurate for slowly-varying density regions, while $F_1(s)$ should describe one- and two-electron systems as well as iso-orbital regions. Eq. (19) represents a simple interpolation between these limits, where the parameter p models the strength of the connection between these limits (i.e. when $p \rightarrow 0$, $z \neq 0$ then $F^{ePC} \rightarrow zF_1(s)$ and when $p \rightarrow \infty$, $z \neq 1$ then $F^{ePC} \rightarrow F_0(s)$). Quite similar expressions have

been considered in meta-GGA exchange functionals using other iso-orbital indicator e.g. [66].

The parameters of $F_1(s)$ have been fitted to best reproduce the SCE values of all one and two-electron atoms in Tab. I (i.e. H, He, two-electron exponential density and three Hooke's atoms), obtaining $a_1 = 0.1$, $a_2 = 0.9342$, $a_3 = 0.22447$. The term s^8 in the denominator ensures that F_1 is a constant at small s ($F_1 \approx a_1 + a_2$ for $s \leq 0.7$) and approaches fast the asymptotic behavior ($F_1 \approx a_1$ for $s \geq 2$). We have found these features to be important for the accuracy of the ePC model for the two-electron systems described in Sec. III. Note that for one-electron systems, $W_\infty[n] = E_x^{EXX} = -U$, while for many-electron systems

$$-U[n] \leq W_\infty[n] \leq E_x^{EXX}[n], \quad (22)$$

where the first inequality occurs from Eq. (11).

On the other hand, $F_0(s)$ dominates for slowly-varying densities (i.e. when s and z are small). The parameter $\kappa = 1 - A_x/A = 0.491$ has been fixed from the condition that $A_x/A \leq F_0(s) \leq 1$, where $A_x = -\frac{3}{4\pi}(3\pi^2)^{1/3}$ is the LDA exchange prefactor. This condition will ensure that, in the slowly-varying density limit, $W_\infty^{ePC}[n] \leq E_x \approx E_x^{LDA}$. Thus, $F_0(s)$ is non-empirical, and when $s \rightarrow 0$, it behaves as

$$F_0(s) \rightarrow 1 - \mu_\infty s^2 + \mathcal{O}(s^6), \quad \text{when } s \rightarrow 0, \quad (23)$$

such that the PC-GE2 is accurately recovered.

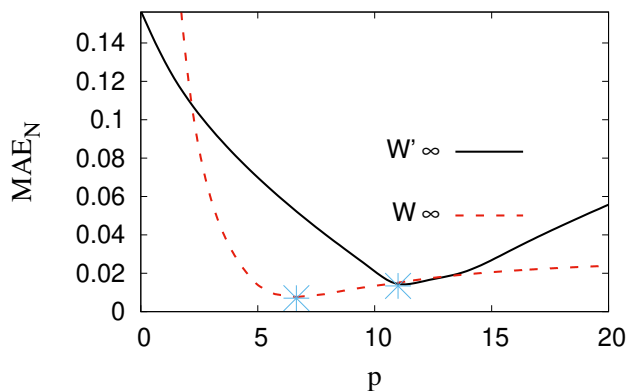


FIG. 1. The mean absolute error per electron MAE_N for $W_\infty^{ePC}(p)$ (red curve) and $W'_\infty^{ePC}(p)$ (black curve), as a function of the parameter p . The minimum error is at $p = 6.65$ for W_∞^{ePC} and at $p = 11$ for W'_∞^{ePC} , respectively.

Finally, in order to find the parameter p , we consider eight atoms for which the W_∞^{SCE} values are known [19, 67] (i.e. Li, Be, B, C, Ne, Ar, Kr and Xe), and we compute the mean absolute error per electron $MAE_N(p) = \frac{1}{8} \sum_{i=1}^8 |W_\infty^{SCE} - W_\infty^{ePC}(p)|/N_i$, where N_i is the number of electrons of the i -th atom. We plot in Fig. 1, MAE_N versus p , and we take $p = 6.65$, where the error is minimum. This choice completes the functional construction for W_∞^{ePC} .

B. The ePC model for W'_∞ :

We consider the functional approximation for W'_∞ of the form

$$W'_\infty{}^{ePC}[n_\uparrow, n_\downarrow] = \int d\mathbf{r} C n^{3/2}(\mathbf{r}) F'^{ePC}(s, z, \zeta), \quad (24)$$

where $C = 1.535$, $\zeta = (n_\uparrow - n_\downarrow)/n$ is the relative spin polarization [56], and

$$\begin{aligned} F'^{ePC}(s, z, \zeta) &= F'_0(s) + \left(z^p F'_1(s, \zeta) - F'_0(s) \right) z^2, \\ F'_1(s, \zeta) &= \left(b_1 + [b_1 + b_2 s^2] e^{-b_3 s^6} \right) (1 - \zeta^{10}), \\ F'_0(s) &= \frac{1 + (\mu'_\infty + 1)s^2}{1 + s^2}. \end{aligned} \quad (25)$$

Similarly to the case of W_∞ , $F'_1(s, \zeta)$ is constructed from two-electron systems, obtaining the parameters $b_1 = 0.04865$, $b_2 = 4.3217$ and $b_3 = 16.581$. Note that for any one-electron system, $F'_1(s, \zeta = 1) = 0$ such that $W'_\infty{}^{ePC}[n_\uparrow, n_\downarrow]$ is exact. By construction, the term $(1 - \zeta^{10})$ is practically important only for $\zeta \geq 0.7$, otherwise F'_1 can be considered independent of spin polarization.

For the slowly-varying density regime, $F'_0(s)$ dominates by construction, and recovers the PC-GE2 as

$$F'_0(s) \rightarrow 1 + \mu'_\infty s^2 + \mathcal{O}(s^4), \quad \text{when } s \rightarrow 0. \quad (26)$$

To find the parameter p , we use the same technique as before. Thus, we consider 5 atoms for which $W'_\infty{}^{SCE}$ is known [18] (i.e. Li, Be, B, C, and Ne) and we compute $MAE_N(p) = \frac{1}{5} \sum_{i=1}^5 |W'_\infty{}^{SCE} - W'_\infty{}^{ePC}(p)|/N_i$, showing it in Fig. 1. The error is minimum at $p = 11$, that completes the functional construction for $W'_\infty{}^{ePC}$.

C. Properties of the ePC model:

The ePC model satisfies the following properties:

- $F^{ePC}(s, z)$ and $F'^{ePC}(s, z, \zeta)$ are analytical functions and do not have any order-of-limits problem (e.g. $\lim_{z \rightarrow 1} \lim_{s \rightarrow 0} F^{ePC} = \lim_{s \rightarrow 0} \lim_{z \rightarrow 1} F^{ePC} = F_1(0)$). We recall that meta-GGA functionals that depend on both meta-GGA ingredients z and $\alpha = (\tau - \tau^W)/\tau^{unif}$, (e.g. TPSS [68] and TM [69] exchange functionals) can have this problem that may cause severe failures [70–72]. Note that in this work we use the bounded iso-orbital indicator z to fulfill the known constraints on W_∞ and W'_∞ . For properties of other iso-orbital indicators, see Refs. [73, 74].
- Under a uniform density scaling $n_\lambda(\mathbf{r}) = \lambda^3 n(\lambda \mathbf{r})$, we have [20, 21]

$$\begin{aligned} W_\infty{}^{ePC}[n_\lambda] &= \lambda W_\infty{}^{ePC}[n], \\ W'_\infty{}^{ePC}[n_\lambda] &= \lambda^{3/2} W'_\infty{}^{ePC}[n]; \end{aligned} \quad (27)$$

- For a slowly-varying density region, where $z \approx (5/3)s^2/[1 + (5/3)s^2]$, the ePC model recovers the PC-GE2 (see Eqs. (13)-(16)):

$$\begin{aligned} W_\infty{}^{ePC}[n] &\rightarrow \int d\mathbf{r} A n^{4/3}(\mathbf{r}) (1 - \mu_\infty s^2 + \mathcal{O}(s^6)), \\ W'_\infty{}^{ePC}[n] &\rightarrow \int d\mathbf{r} C n^{3/2}(\mathbf{r}) (1 + \mu'_\infty s^2 + \mathcal{O}(s^4)). \end{aligned} \quad (28)$$

We recall that $W_\infty{}^{PC}$ [20, 21], $W_\infty{}^{mPC}$ [47], $W_\infty{}^{hPC}$ [50] also behave as $W_\infty{}^{PC-GE2}$ at small reduced gradients s . On the other hand, $W_\infty{}^{PC-GE2}$ is recovered in the slowly-varying density limit only by $W'_\infty{}^{ePC}$, while all the other known models ($W_\infty{}^{PC}$, $W_\infty{}^{mPC}$, $W_\infty{}^{hPC}$, $W_\infty{}^{MGGA}$ of Ref. [20, 21]) fail to fulfill this exact constraint.

Instead, for a constant density, all these models yield the LDA behavior: $W_\infty{}^{LDA}[n] = \int d\mathbf{r} A n^{4/3}(\mathbf{r})$ and $W'_\infty{}^{LDA}[n] = \int d\mathbf{r} C n^{3/2}(\mathbf{r})$;

- The negativity and positivity conditions, respectively:

$$\begin{aligned} W_\infty{}^{ePC}[n] &\leq 0, \\ W'_\infty{}^{ePC}[n] &\geq 0. \end{aligned} \quad (29)$$

Note that PC and hPC models fail for both of these conditions, while mPC and meta-GGA models satisfy them. Moreover, the tighter bound $W_\infty[n] \leq E_x^{EXX}[n]$ still holds for mPC and meta-GGA models, while by construction $W_\infty{}^{ePC}[n] \leq E_x^{LDA}[n]$.

- In the strong-interaction limit of a many-electron system (where in most energetic regions $z \leq 0.5$), the electrons are usually well separated, such that they perform zero-point oscillations around equilibrium positions in a Wigner crystal [19–21, 30]. Consequently, in this case, both W_∞ and W'_∞ must be spin-independent.

On the other hand, in the strong-interaction limit of a few-electron systems (where $z \geq 0.5$), the spin dependence can still be important, for example, to correctly describe spin-polarized small systems, as H and Li atoms. However, $W_\infty[n]$ can be constructed as a functional of the total density, being spin-independent, but still accurate for H and Li atoms (as reported in Table I for PC [20, 21], hPC [50] and ePC models). On the other hand, W'_∞ should vanish for H atom, and this condition requires a spin-dependence of the functional (i.e. $W'_\infty[n_\uparrow, n_\downarrow]$). Then the ePC model satisfies

$$\begin{aligned} W_\infty{}^{ePC}[n_\uparrow, n_\downarrow] &= W_\infty{}^{ePC}[n_\uparrow + n_\downarrow], \quad \text{for } 0 \leq z \leq 1 \\ W'_\infty{}^{ePC}[n_\uparrow, n_\downarrow] &\approx W'_\infty{}^{ePC}[n_\uparrow + n_\downarrow], \quad \text{for } z \leq 0.5. \end{aligned} \quad (30)$$

These conditions are violated by the meta-GGA models [20, 21, 56].

- ePC is exact for the H atom (where $z = 1$ and $\zeta = 1$)

$$\begin{aligned} W_\infty^{ePC} &= -0.3125, \\ W_\infty'^{ePC} &= 0. \end{aligned} \quad (31)$$

We recall that for any one-electron system, $W_\infty = E_x^{EXX} = -U$. Even if this fully-nonlocal constraint cannot be recovered by semilocal functionals [75], the meta-GGA approximations can be accurate for many one-electron systems. On the other hand, $W_\infty' = 0$, an exact condition that is fulfilled by the ePC model.

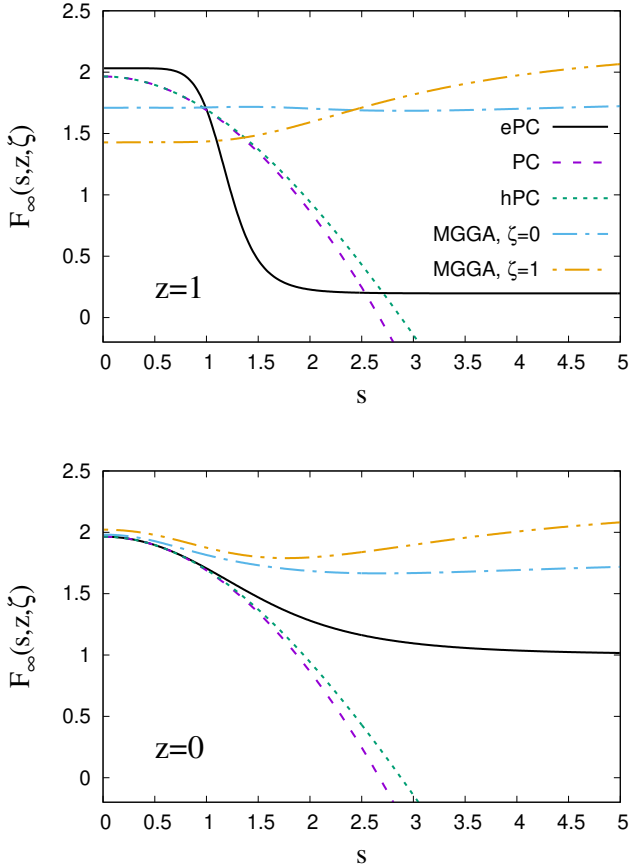


FIG. 2. The enhancement factor $F(s, z, \zeta)$ of the W_∞ , for $z = 1$ (upper panel) and $z = 0$ (lower panel) versus the reduced gradient s , in case of several models (ePC, PC, hPC and meta-GGA).

Now, let us consider the following definitions for the enhancement factors

$$\begin{aligned} F_\infty(s, z, \zeta) &= \frac{w_\infty(n_\uparrow, n_\downarrow, \nabla n_\uparrow, \nabla n_\downarrow, \tau_\uparrow, \tau_\downarrow)}{e_x^{unif}(n)} \\ F_\infty'(s, z, \zeta) &= \frac{w_\infty'(n_\uparrow, n_\downarrow, \nabla n_\uparrow, \nabla n_\downarrow, \tau_\uparrow, \tau_\downarrow)}{w_\infty'^{unif}(n)}, \end{aligned} \quad (32)$$

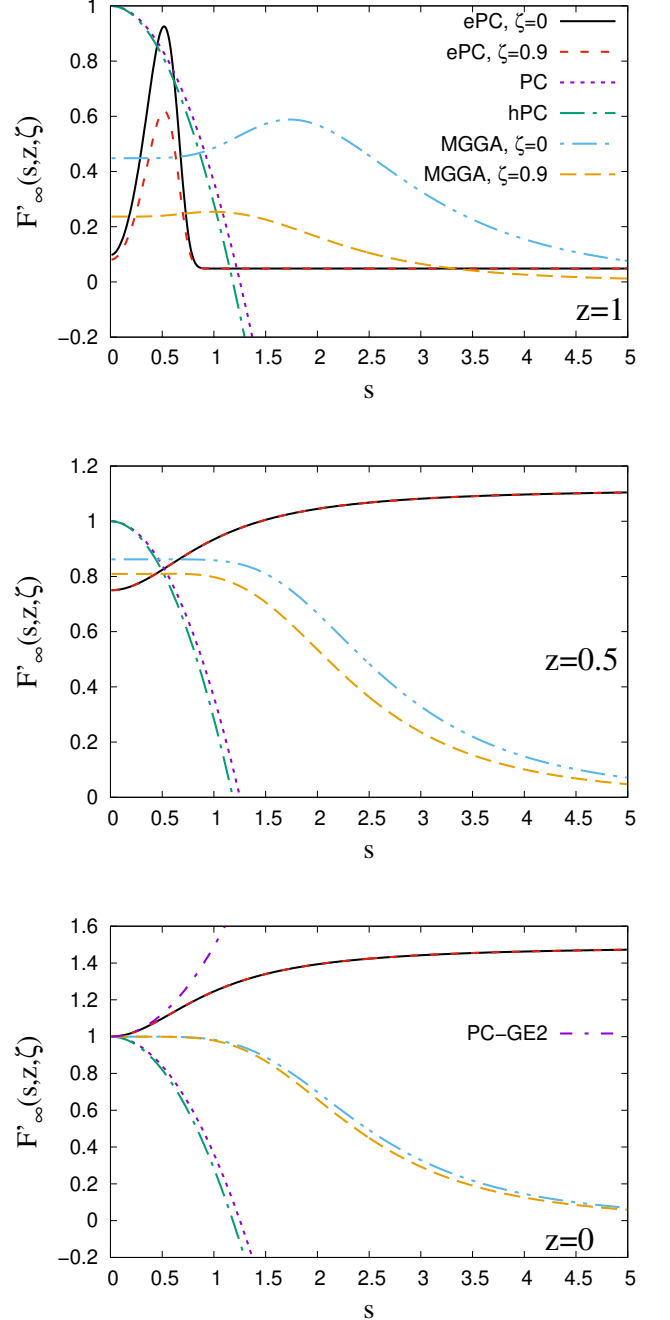


FIG. 3. The enhancement factor $F_\infty'(s, z, \zeta)$ of the W_∞' , for $z = 1$ (upper panel), $z = 0.5$ (middle panel) and $z = 0$ (lower panel) versus the reduced gradient s , in case of several models (ePC, PC, hPC and meta-GGA).

where $e_x^{unif}(n) = A_x n^{4/3}$ is the exchange energy density of a spin-unpolarized uniform electron gas, and $w_\infty'^{unif}(n) = Cn^{3/2}$.

In Fig. 2, we show a comparison between the enhancement factors of several models for W_∞ . We observe that $F_\infty^{PC}(s)$ and $F_\infty^{hPC}(s)$ are positive for $s \lesssim 2.68$ and

$s \lesssim 2.88$, respectively, while for larger values of reduced gradients, both $F_{\infty}^{PC}(s)$ and $F_{\infty}^{hPC}(s)$ are negative. On the other hand, $F_{\infty}^{ePC}(s, z)$ and $F_{\infty}^{MGGA}(s, z, \zeta)$ are positive for any s, z , and ζ . In case of $z = 1$ (upper panel), $F^{ePC} \approx a_1$ for $s \geq 2.2$, but when z decreases, F^{ePC} becomes more uncompressed, as shown for the $z = 0$ (lower panel) where $F^{ePC} \approx 1$ for $s \geq 4$. Finally, we mention that F^{MGGA} is significantly dependent on ζ , for any value of z . This failure is not present in the other models.

In Fig. 3, we show the enhancement factors of several models for W'_{∞} . Now, $F'^{PC}(s)$ and $F'^{hPC}(s)$ are positive only for $s \lesssim 1.25$ and $s \lesssim 1.18$, respectively. Regarding the ePC model, we observe that at $z = 1$ it starts from $2b_1(1 - \zeta^{10})$ at $s = 0$, showing a sharp peak (whose magnitude is ζ -dependent) at $s \approx 0.5$, and at $s \gtrsim 0.9$ rapidly approaches the constant asymptote b_1 .

On the other hand, for $z = 0.5$ (middle panel) and $z = 0$ (lower panel), $F'^{ePC}(s, z, \zeta)$ is almost independent of the relative spin-polarization, by construction, correcting the behavior of the meta-GGA. Note that at $z = 0$, $F'^{ePC}(s, z, \zeta)$ recovers PC-GE2 for $s \lesssim 0.7$ and increases monotonically from 1 to $1 + \mu'_{\infty}$, being very different from all the other models.

III. APPLICATIONS TO ATOMS, MODEL SYSTEMS AND H₂ DISSOCIATION:

A. Atoms

In Table I, we report the W_{∞} and W'_{∞} results for atoms. The SCE reference values were taken from Refs. [18, 19, 50, 53, 54, 67]. W_{∞}^{ePC} and W_{∞}^{TPSS} give the best results (with $\text{MAE}_N = 5.5 \cdot 10^{-3}$ and $5.7 \cdot 10^{-3}$) closely followed by W_{∞}^{hPC} , while W_{∞}^{PC} has larger errors. Nevertheless, we mention that W_{∞}^{PC} is significantly better than W_{∞}^{mPC} , W_{∞}^{PBE} or W_{∞}^{LDA} , see Refs. 20, 21, and 53. We also note that for heavier atoms (Ar, Kr, and Xe), all functionals are less accurate, W_{∞}^{TPSS} yielding the best performance. In particular, for the Ar atom, W_{∞}^{ePC} gives the worst result, with $\text{MAE}_N = 0.02$.

On the other hand, in case of W'_{∞} , ePC ($\text{MAE}_N = 9 \cdot 10^{-3}$) is by far the most accurate, with a MAE_N 2-7 times better than all other methods. For He to Ne atoms, we see that the PC and TPSS overestimate while hPC and ePC are significantly more accurate. For the heavier atoms (Ar, Kr, Xe), the differences between the model predictions are quite substantial, such that SCE benchmark calculations are needed to understand the performance of these models for heavy atoms.

In order to visualize the ePC behavior, we also show in Fig. 4, the enhancement factors F_{∞} and F'_{∞} for the Ne atom. We observe that both F_{∞}^{ePC} and F'_{∞}^{ePC} are quite close to PC and hPC for $r \leq 2$ and $r \leq 1.5$, respectively. At larger distances from the nucleus, the ePC model behaves smoothly and approaches a positive constant (in

TABLE I. W_{∞} and W'_{∞} (in a.u.) for several atoms and spherical model systems (Hooke's atom with three values of ω : 0.5, 0.1, and 0.036) [50] and the two-electron exponential density $n(r) = 2/\pi e^{-2r}$ (Exp.). For atoms we use the EXX orbitals and densities, while for the model systems we use the exact orbitals and densities. Last lines of each panel show the mean absolute error (MAE) and the mean absolute error per electron MAE_N . Best results are in boldface.

	SCE	PC	hPC	ePC	TPSS
	W_{∞}				
H	-0.3125	-0.313	-0.329	-0.3125	-0.3125
Hook(0.5)	-0.743	-0.702	-0.743	-0.758	-0.754
Hook(0.1)	-0.304	-0.284	-0.303	-0.311	-0.308
Hook(0.036)	-0.170	-0.156	-0.167	-0.174	-0.170
Exp.	-0.910	-0.886	-0.906	-0.913	-0.917
He	-1.500	-1.463	-1.492	-1.498	-1.512
Li	-2.603	-2.558	-2.582	-2.600	-2.590
Be	-4.021	-3.943	-3.976	-4.020	-3.980
B	-5.706	-5.643	-5.676	-5.756	-5.660
C	-7.782	-7.714	-7.753	-7.853	-7.710
Ne	-20.035	-20.018	-20.079	-20.035	-19.979
Ar	-51.555	-51.547	-51.615	-51.191	-51.380
Kr	-166.850	-167.356	-167.438	-166.539	-166.776
Xe	-322.835	-324.521	-324.619	-323.346	-323.344
MAE	-	0.186	0.188	0.096	0.073
MAE _N	-	0.0125	0.0079	0.0055	0.0057
	W'_{∞}				
H	0	0.043	0.025	0	0
Hook(0.5)	0.208	0.215	0.208	0.215	0.240
Hook(0.1)	0.054	0.054	0.053	0.053	0.062
Hook(0.036)	0.022	0.021	0.021	0.020	0.026
Exp.	0.293	0.344	0.308	0.333	0.339
He	0.621	0.729	0.646	0.636	0.728
Li	1.38	1.622	1.434	1.448	1.528
Be	2.59	2.919	2.600	2.624	2.713
B	4.2	4.694	4.244	4.270	4.405
C	6.3	7.079	6.475	6.429	6.683
Ne	22	24.425	23.045	21.997	23.835
Ar	-	86.17	82.59	79.854	86.76
Kr	-	381.01	370.34	376.26	390.99
Xe	-	886.3	866.05	894.27	914.2
MAE	-	0.407	0.127	0.034	0.263
MAE _N	-	0.069	0.019	0.009	0.042

the asymptotic limit, the density decays exponentially, such that $s \rightarrow \infty$ and $z \rightarrow 1$, then $F_{\infty}^{ePC} \approx a_1$ and $F'_{\infty}^{ePC} \approx b_1$). The asymptotic behaviors of F_{∞} and F'_{∞} in the SCE approach (see Eq. (11)) using the conventional gauge [76], is an open problem that is not investigated in this work. Here we only mention that F_{∞}^{MGGA} takes the maximum value allowed by locally satisfying the Lieb-Oxford bound; however, all the models shown in the figure (ePC, hPC, PC, and MGGA) satisfy the Lieb-Oxford bound [77], which in the SCE limit becomes $W_{\infty} \geq -1.68 \int dr n(\mathbf{r})^{4/3}$.

Then, we considered the total energies of atoms as computed using the genISI2 ACII approach [54]. In Tab. II we report the results of the TE18 benchmark [78], which represents the H-Ar atoms. We use the nearly

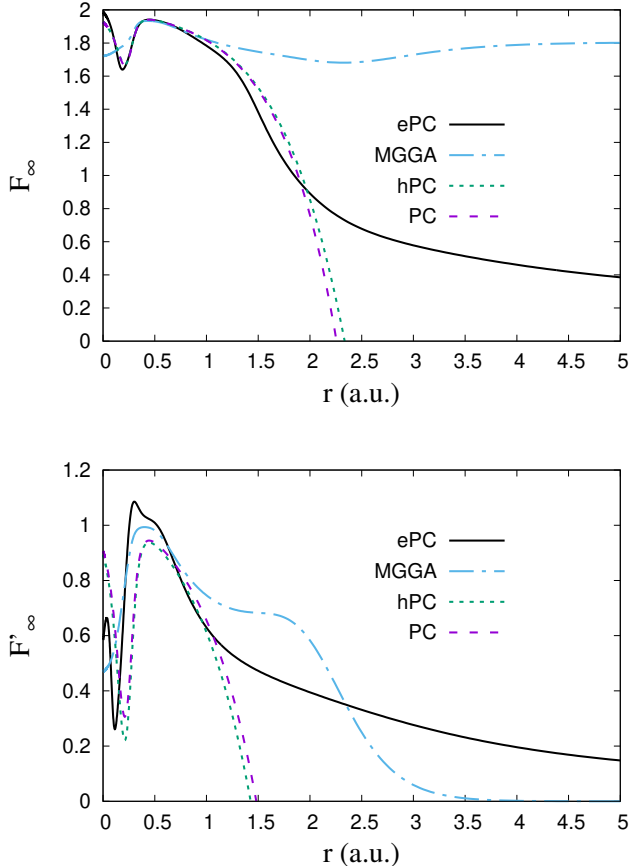


FIG. 4. The enhancement factors F_∞ (upper panel) and F'_∞ (lower panel) versus the radial distance from the nucleus r , for the Ne atom.

complete 5ZaPa-NR-CV basis-set [79]; the reference data is the CCSD(T) in the same basis-set[78]. (For more computational details, see Sec. V.) We considered effective exact-exchange orbitals [80, 81]. The results show that while GL2 strongly overestimates the total energy, genISI2 gives an overall accuracy of only 3-4 mHa. Such accuracy is even superior to the one of HFAC24 functional (5 mHa)[78]. Moreover, the ePC results with MAE=3.4 mHa are slightly better than the hPC ones. Note that for the same benchmark, MP2 has MAE of 15.8 mHa [78]. For comparison with other popular functionals, see Table 2 of Ref. [78].

B. Two-electron model density:

Let us consider the following $2e^-$ spherical density

$$n_\beta(r) = \frac{4(\beta^2 + 1)^3}{(\beta^6 + 3\beta^4 + 2)\pi} e^{-2r} \cos^2(\beta r), \quad (33)$$

such that for any value of β , the normalization condition is $\int_0^\infty dr 4\pi r^2 n_\beta(r) = 2$. Note that when $\beta = 0$ then the

TABLE II. Reference CCSD(T) total energy (in mHa) and the errors (approx. -reference) of GL2, genISI2-hPC, genISI2-ePC and genISI2-TPSS functionals for the TE18 test. The mean error (ME) and MAE (in mHa) are also reported.

	Ref.	GL2	genISI2 hPC	genISI2 ePC	genISI2 TPSS
H	-500.000	0.004	0.004	0.004	0.004
He	-2903.233	-5.816	0.590	-0.073	1.227
Li	-7477.612	-4.064	-0.241	-0.656	0.366
Be	-14666.741	-30.200	-1.987	-3.835	-0.845
B	-24652.573	-28.964	0.367	-2.858	1.646
C	-37842.983	-30.189	1.860	-1.570	3.687
N	-54586.561	-32.770	2.580	-0.772	5.011
O	-75062.803	-45.726	4.156	0.487	7.048
F	-99727.414	-62.887	3.170	-0.217	7.076
Ne	-128929.226	-82.816	0.083	-2.599	5.177
Na	-162246.996	-67.001	1.582	0.371	6.591
Mg	-200045.220	-80.468	-3.013	-3.386	2.445
Al	-242337.543	-78.090	-2.280	-2.421	3.158
Si	-289349.212	-82.588	-4.075	-3.873	1.544
P	-341248.082	-91.377	-7.910	-7.274	-2.017
S	-398097.957	-100.467	-7.724	-6.581	-1.509
Cl	-460135.451	-115.610	-11.024	-9.307	-4.275
Ar	-527527.142	-134.179	-16.634	-14.311	-9.263
ME		-59.623	-2.250	-3.271	1.504
MAE		59.623	3.849	3.366	3.494

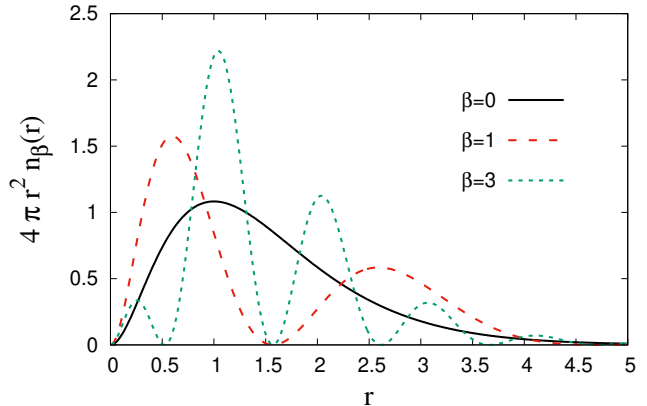


FIG. 5. The radial density $4\pi r^2 n_\beta(r)$ of the two-electron model density in Eq. (33), versus the radial distance r , for several values of the β parameter ($\beta = 0, 1$ and 3).

$2e^-$ exponential density is found. In Fig. 5, we plot this density for several values of the β frequency.

Note that the SCE values were computed using the method presented in Ref. 82.

This model system is a very hard test for the PC and hPC models. As shown in Fig. 6, PC and hPC start to fail even at relatively small values of β . In particular for $W'[n_\beta]$, PC and hPC give the wrong sign for $\beta > 1$. On the other hand, both ePC and TPSS models are remarkably accurate, validating our construction for $F_1(s)$ and $F'_1(s, \zeta)$, see Eqs. (21) and (25).

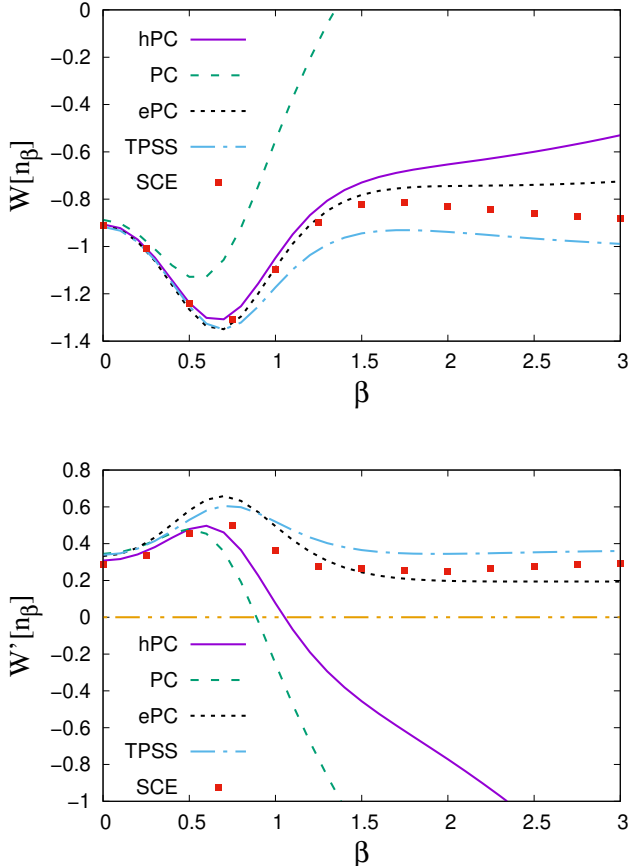


FIG. 6. The strong-interaction functionals $W[n_\beta]$ (upper panel) and $W'[n_\beta]$ (lower panel) versus the β parameter for the two-electron model density of Eq. (33).

C. The s and p hydrogenic shells:

As another example, let us consider the hydrogenic orbitals $\psi_{nlm}(\mathbf{r}, Z) = R_{nl}(r, Z)Y_{lm}(\theta, \phi)$, that were used to investigate the nuclear [83] and asymptotic regions [84] in atoms, as well as the large atoms in the strong-interaction limit [67]. Here $R_{nl}(r, Z)$ are the normalized radial functions, Z is the nuclear charge, $Y_{lm}(\theta, \phi)$ are the spherical harmonics, and n, l, m are the principal, angular momentum and azimuthal quantum numbers, respectively. The density of the fully filled nl shell is

$$\rho_{nl}(r, Z) = \frac{(2l+1)}{2\pi} |R_{nl}(r, Z)|^2, \quad (34)$$

and we consider neutral s ($l = 0$, $Z = N = 2$) and p ($l = 1$, $Z = N = 6$) shells.

In Fig. 7, we show the radial densities ($4\pi r^2 \rho_{nl}$) for the p -shells ($l = 1$) and $n = 2, 3$ and 4. We observe that when n increases, the density becomes more diffuse, similar to the real valence densities from pseudopotential calculations.

In Figs. 8 and 9 we report the strong-interaction func-

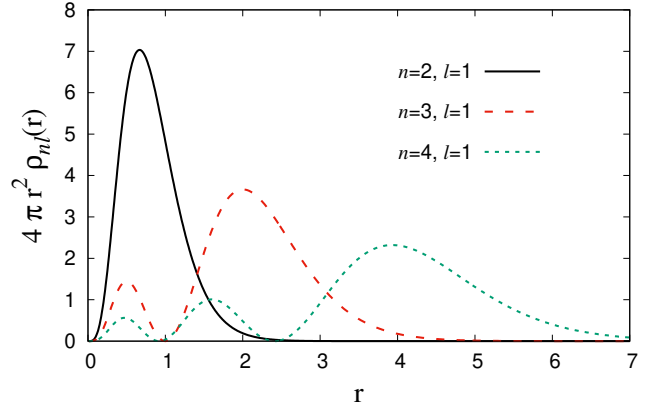


FIG. 7. The radial densities of the fully filled p -shells (see Eq. (34)) versus the radial distance r . The area under each curve is the number of electrons ($N = 6$).

tionals W_∞ and W'_∞ as a function of the principal quantum number n , for the s - and p -shells, respectively. In case of the s -shell, we also compute the SCE values [82].

The ePC and meta-GGA models are accurate, yielding the correct behavior for all values of n . On the other hand, the hPC and PC functionals show an incorrect sign for increasing n , as also in the two-electron model density in the previous subsection. The hPC improves considerably over the PC, especially for W_∞ , which becomes positive only at very large n .

The s - and p -hydrogenic shell models can be of interest to describe atoms with pseudopotential. In fact, in this case the density at the atomic core can be zero, and the results presented here show that while PC and hPC can give even a wrong sign in those cases, this is not the case for ePC.

D. Quasi-two-dimensional infinite barrier model (quasi-2D IBM):

Let us consider the quasi-2D IBM quantum well of thickness L in the z -direction [85–89]. The true 2D uniform electron gas limit is recovered by shrinking the z -coordinate, keeping fixed the total number of electrons per unit area (n^{2D}). The quasi-2D regime is obtained when $L \leq \sqrt{3/2\pi} r_s^{2D} = L_{\max}$ [85], being equivalent to a non-uniform scaling in one dimension (i.e. $n_\lambda^z(x, y, z) = \lambda n(x, y, \lambda z)$, with $\lambda = L_{\max}/L$).

Most of the semilocal functionals fail severely for the quasi-2D IBM, which represents a dimensional crossover, from 3D to 2D. Recently, we have shown that the ACII functionals are remarkably accurate for the quasi-2D IBM when the “exact” expressions for $W_\infty(L)/N$ and $W'_\infty(L)/N$ are used, which were constructed from a simple interpolation between the 2D and 3D expressions (see Eqs. (21) and (23) of Ref. [54]).

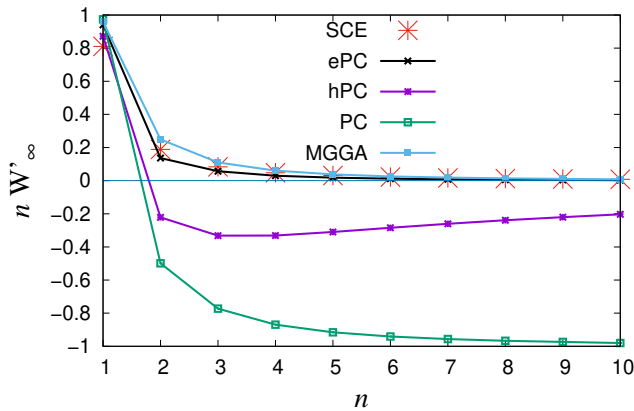
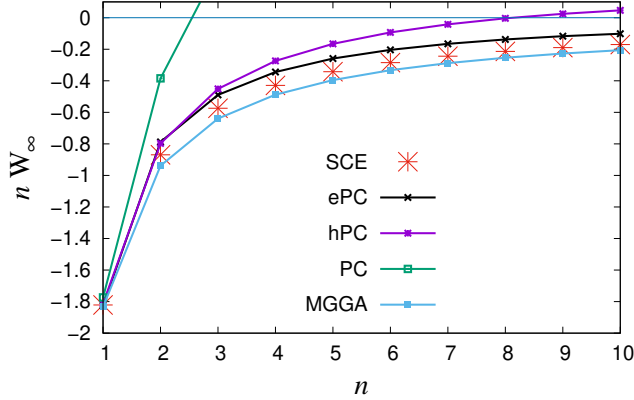


FIG. 8. W_∞ (upper panel) and W'_∞ (lower panel) multiplied with the principal quantum number n , versus n , for the s -hydrogenic neutral shells (see Eq. (34) with $l = 0$, $Z = N = 2$).

In Fig. 10, we show the performance of the ePC model for the quasi-2D IBM with the 2D bulk parameter $r_s^{2D} = 3$. Note that similar results have been also found for $r_s^{2D} = 1$ and $r_s^{2D} = 5$. We observe that $W_\infty^{ePC}(L)/N$ is remarkably accurate for $L/L_{\max} \geq 0.1$, outperforming both hPC and MGGA. Note that $W_\infty(L)^{hPC}/N \leq E_x^{EXX}/N$ at $L/L_{\max} \leq 0.1$, failing badly and even becoming positive at $L/L_{\max} \leq 0.05$. Also $W_\infty(L)^{MGGA}/N$ diverges when $L/L_{\max} \rightarrow 0$.

Moreover, ePC also improves significantly over MGGA for $W'_\infty(L)/N$, while hPC fails drastically. Overall, we think that the ePC performs encouragingly for the dimensional crossover, and it can be safely used in real quasi-2D calculations (e.g. two-dimensional materials [90] and interfaces [91]), where the strength of the quasi-2D regime is usually comparable with the case of quasi-2D IBM when $L/L_{\max} \rightarrow 0.3$.

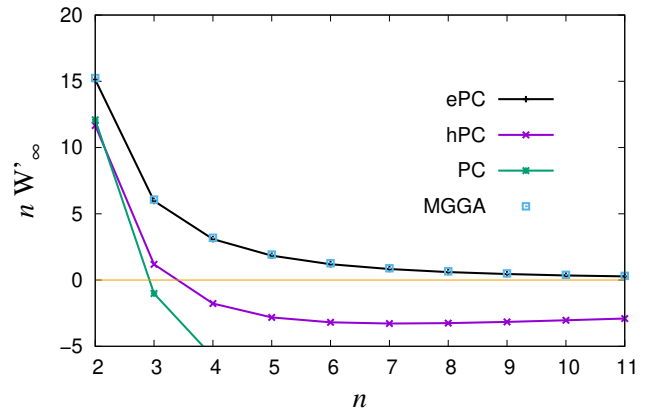
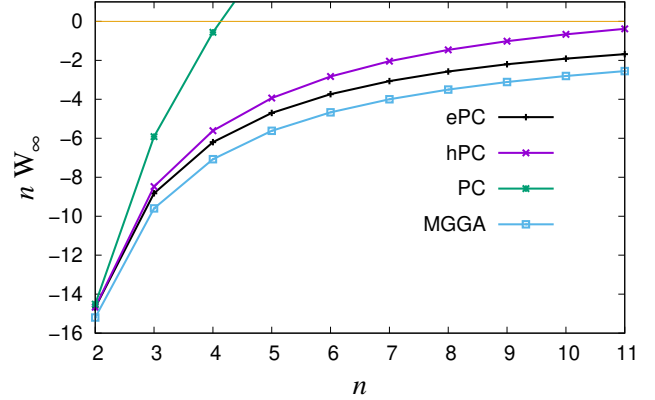


FIG. 9. Same as Fig. 8, but for the p -hydrogenic neutral shells (see Eq. (34) with $l = 1$, $Z = N = 6$).

E. Perturbed uniform electron gas (UEG):

Now let us consider a perturbed UEG in the x -direction, with the density

$$n(x) = n_0 + \delta n(x) = n_0 \left[1 + A \cos(\beta x) \right], \quad (35)$$

where $n_0 = 3/(4\pi r_s^3)$ and we take $A = 1/10$, then the perturbation density $\delta n(x, y, z)$ is small. Such a system is translationally invariant in the (yz) -plane. In Fig. 11, we show $n(x)$ versus x for bulk parameters $r_s = 2$ and 3, and for $\beta = 1$ and 3, respectively. Note that at $\beta = 1$ the density varies slowly, while at $\beta = 3$ there are small-amplitude, short-wavelength density waves, where the kinetic energy density is $\tau \rightarrow \tau^{TF} + \tau^W$ [92], such that the meta-GGA ingredient is

$$z = (5s^2/3)/(1 + (5s^2/3)).$$

We take x in the interval $0 \leq x/\lambda_F \leq 1$, where $\lambda_F = 2\pi/k_F$ is the bulk Fermi wavelength, with $k_F = (3\pi^2 n_0)^{1/3}$ being the Fermi bulk wavevector, and $r_s = 2$. For such a system, the TPSS correlation energy is very accurate, and we consider it as the reference correlation.

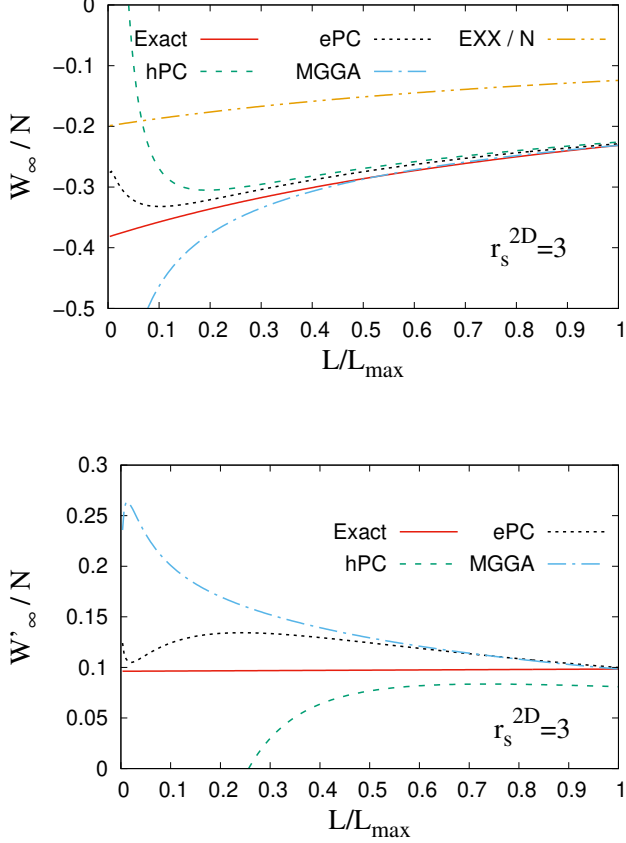


FIG. 10. $W_\infty(L)/N$ (upper panel) and $W'_\infty(L)/N$ (lower panel) from hPC, ePC and MGGA models, for the quasi-2D IBM with the 2D bulk parameter $r_s^{2D} = 3$. The reference curves are taken from Ref. [54].

On the other hand, the GL2 correlation diverges so the ACII correlation functionals depend only on E_x^{EXX} , W_∞ and W'_∞ .

First, we compute the ISI, revISI and genISI correlation energies per unit area E_c , within the ePC model, and the results are reported in the upper panel of Fig. 12. ISI and revISI significantly underestimate the correlation energy, whereas the genISI, which has been constructed from the UEG reference system, achieves good accuracy. We have also obtained similar patterns in the cases of UEG and jellium clusters [52].

Finally, in the lower panel of Fig. 12 we show the genISI correlation energy per unit area E_c computed using PC, hPC, ePC, and meta-GGA models, such that we can make a fair comparison between these models. ePC, PC and hPC are accurate, better than the meta-GGA that induces a slightly higher correlation energy.

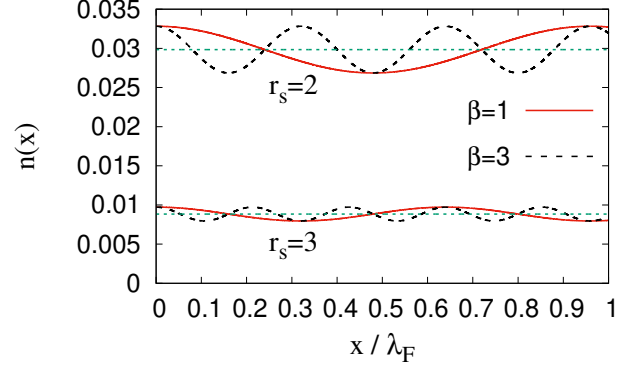


FIG. 11. The density $n(x)$ (see Eq. (35)) versus the scaled distance x/λ_F for bulk parameters $r_s = 2$ and 3, and for several values of the frequency β .

F. H_2 dissociation

In Fig. 13, we show the H_2 dissociation curve within a spin-restricted formalism, a system that becomes a prototype example for the static correlation present in stretched molecular bonds and the dissociation limit [54, 93–99]. The performance of the ACII XC functionals for this system has been recently investigated, e.g. see Refs. [50, 54, 78], such that here we comment only on the comparison between genISI2-hPC and genISI2-ePC, computed with EXX orbitals. They agree closely until $R \approx 7$ bohr, where the use of hPC gives a repulsive bump, which is mostly attenuated in the case of ePC curve. At the dissociation limit $D = E[H_2] - 2E[H]$ is closer to exact for hPC than for ePC. The better behavior of the hPC is due to an error cancellation between the positive and negative regions of F_∞^{hPC} , such that $0 = W_\infty^{SCE} \leq W_\infty^{hPC} \leq W_\infty^{ePC}$. We also observe that genISI2-ePC is superior in this limit to the HFAC24 functional [78].

Obtaining $W_\infty^{ePC} = 0$ for the spin-restricted hydrogen atom with half spin-up and half spin-down electrons, $H(1/2, 1/2)$, is not possible at the meta-GGA level, with the enhancement factor non-negativity condition, as for this system $z = 1$ and $\zeta = 0$, like all two-electrons atoms, where W_∞^{ePC} is not zero. Approaches beyond meta-GGAs are required.

Concerning W_∞ , we have that, using exact orbitals (instead of EXX), $W_\infty/2 = -0.3128, -0.3292, -0.3124, -0.3639$ a.u., for PC, hPC, ePC and TPSS, respectively, to be compared with the exact $W_\infty/2 = -0.3125$ a.u. Thus only PC and ePC give very accurate values.

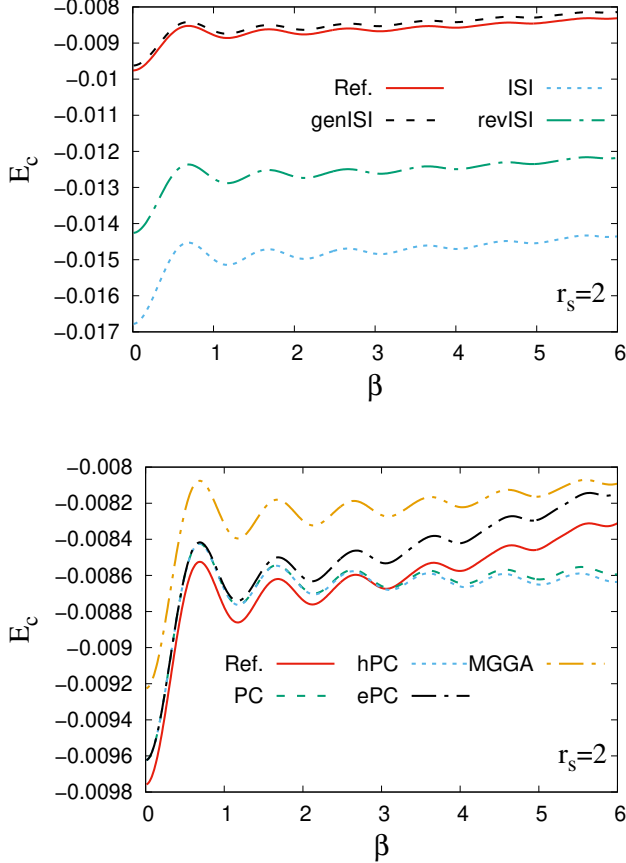


FIG. 12. Upper panel: ISI, revISI and genISI correlation energies per unit area E_c , for the perturbed UEG of Eq. (35), as a function of the frequency β . The reference is the TPSS correlation energy. The ACII functionals use the ePC model. Lower panel: genISI correlation energy per unit area E_c computed using PC, hPC, ePC, and meta-GGA models for the strong-interaction functionals, for the perturbed UEG of Eq. (35), as a function of the frequency β . The reference is the TPSS correlation energy.

IV. APPLICATION TO ATOMIZATION ENERGIES AND IONIZATION POTENTIALS:

A. Optimized hybrid orbitals:

The ACII XC methods are pure KS DFT approach, so that they must be based on the optimized effective potential (OEP) self-consistent KS orbitals.[50], The impact of the ground-state KS orbitals over the different ACII ingredients has been investigated in Ref. 54 and it was found that the GL2 terms strongly depend on the KS orbitals (in particular on the KS gap).

Self-consistent correlated OEP calculations, although possible [50], are numerically cumbersome, thus exchange-only OEP (OEPx) orbitals are usually used for the ACII functionals [54], because they are close to the exact KS orbitals for finite systems, such as atoms [54]

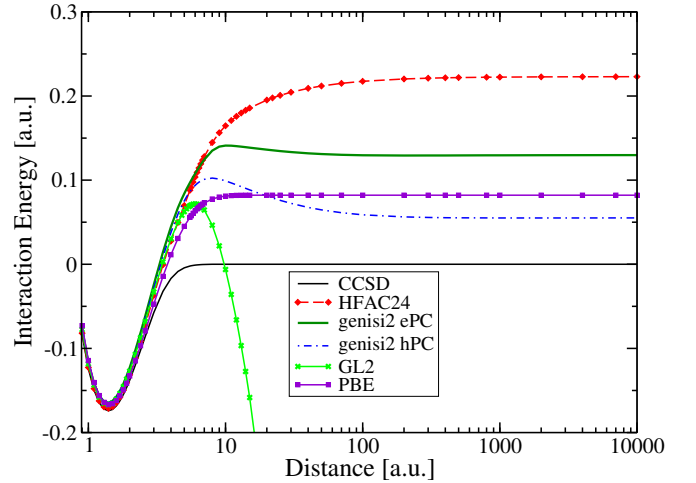


FIG. 13. H_2 dissociation curve within a spin-restricted formalism. GL2 and genISI2 using EXX orbitals, while the HFAC24 is based on HF orbitals. The exact and PBE curves are also shown.

and small molecules, where the correlation potential decays much faster in vacuum than the OEPx potential [60, 100]. Nevertheless, OEPx orbitals are quite challenging for large systems, too. In this work, we propose a simple optimized hybrid approach (in the generalized Kohn-Sham scheme) in place of OEP, in order to compare hPC and ePC in standard molecular benchmarks.

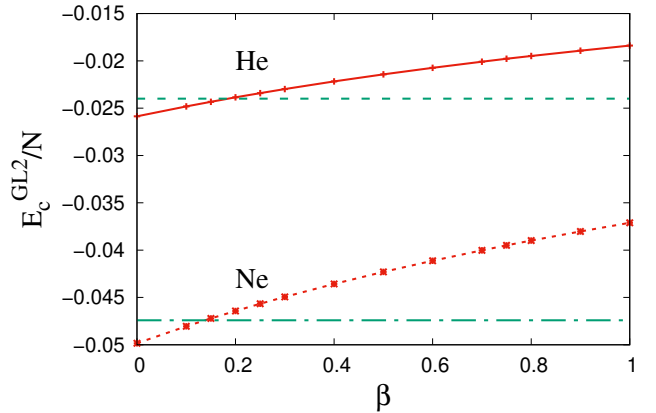


FIG. 14. The GL2 correlation per electron E_c^{GL2}/N computed using the hybrid PBE orbitals with a fraction β of non-local Hartree-Fock-like exchange, for He and Ne atoms. Also shown are the reference GL2 correlation energies (taken from Ref. 54).

We consider the self-consistent orbitals obtained from the hybrid PBE XC functional [101]

$$E_{xc}[n](\beta) = \beta E_x^{HF}[n] + (1-\beta)E_x^{PBE}[n] + E_c^{PBE}[n], \quad (36)$$

where the fraction β of Hartree-Fock (HF)-like exchange $E_x^{HF}[n]$ needs to be optimized to obtain the exact GL2 correlation energy (see Table III of Ref. 54). In

this hybrid scheme, the corresponding GL2 correlation energy is:

$$E_c^{GL2}[\{\phi_a, \epsilon_a\}] = E_c^{MP2}[\{\phi_a, \epsilon_a\}] - (1 - \beta) \sum_{i,b} \frac{|\langle \phi_i | \hat{v}_x^{PBE} - \hat{v}_x^{HF} | \phi_b \rangle|^2}{\epsilon_b - \epsilon_i}, \quad (37)$$

where i, b indicate the occupied and virtual orbitals, respectively; and $\hat{v}_x^{PBE}, \hat{v}_x^{HF}$ are the local PBE and non-local HF -like exchange potentials, respectively.

In Fig. 14 we show E_c^{GL2} as a function of the parameter β , for He and Ne atoms. The horizontal lines represent the exact GL2 correlation energies [54]. We observe that in both cases, for $\beta \approx 0.15$, the GL2 correlation is close to exact. Thus, for molecular calculations, we use the orbitals from the functional in Eq. (37), with $\beta = 0.15$ (for simplicity we name this functional PBE15).

B. Atomization energies and ionization potentials

TABLE III. Reference atomization energies (in kcal/mol) and the errors (approx.-reference) of PBE, GL2, genISI2-hPC and genISI2-ePC functionals for the AE6 test. The mean error (ME) and MAE (in kcal/mol) and MARE (in %) are also reported. PBE15, GL2 and genISI2 all use PBE15 self-consistent orbitals. Reference values are from Ref. [102] and the basis-set is 5ZaPa-NR-CV[79].

	Ref.	PBE	PBE15	GL2	genISI2 hPC	genISI2 ePC
SiH ₄	324.59	-10.93	-9.71	13.43	-7.43	-6.81
SiO	193.40	3.33	-4.67	91.50	30.39	30.86
S ₂	103.90	11.52	6.59	46.68	17.50	17.30
C ₂ H ₂ O ₂	635.33	27.91	10.46	159.42	13.58	22.22
C ₃ H ₄	705.28	15.57	7.61	97.86	-0.63	7.70
C ₄ H ₈	1150.12	17.41	11.02	112.74	-12.96	-1.03
ME		10.80	3.55	86.94	6.74	11.71
MAE		14.45	8.34	86.94	13.75	14.32
MARE		4.05	2.57	24.19	6.37	6.56

We employ the hPC and ePC strong-interaction models, in the genISI2 ACII XC functional [54], for two standard molecular benchmarks. Calculations have been done in a nearly complete basis-set (see Computational Details section) in order to avoid basis-set inaccuracies for the calculation of the GL2 correlation energy [78].

In Table III we report the atomization energies of molecules from the popular benchmark test AE6 [102, 106]. GL2 strongly overestimates the atomization energies of all AE6 molecules, with MAE \approx 90 kcal/mol, almost one order of magnitude worse than MP2 [106]. We recall that the main difference between GL2 and MP2 is given by the type of orbitals, as the HOMO-LUMO gap from the PBE15 orbitals is considerably smaller than the gap from the HF orbitals. On the other hand, genISI2 strongly improves over GL2, with MAE \approx 14 kcal/mol, which is close to the PBE one. Comparing

TABLE IV. Reference ionization potential(Ref.), and the errors obtained from PBE, PBE15, GL2, genISI2-hPC and genISI2-ePC, for the G21IP benchmark test (but hydrogen atom) [103–105]. The last rows show the error statistics; the mean error (ME), MAE and MARE (in %). All the results are in kcal/mol. PBE15, GL2 and genISI2 all use PBE15 self-consistent orbitals. Reference values are from Ref. [105] and the basis-set is 5ZaPa-NR-CV[79].

Sys.	Ref.	PBE	PBE15	GL2	genISI2 hPC	genISI2 ePC
Li	123.30	5.58	5.33	1.17	1.08	1.34
Be	214.90	-7.37	-7.73	9.17	-2.99	-2.14
B	190.40	9.64	9.25	1.99	1.19	2.00
C	259.60	6.54	6.15	3.47	0.24	0.52
N	335.30	4.39	3.97	6.03	0.72	1.13
O	313.80	10.48	7.47	12.86	-0.86	-0.07
F	401.70	5.41	2.44	18.78	1.25	1.84
Na	118.50	5.10	4.17	1.40	-0.11	-0.26
Mg	176.30	-0.76	-1.75	9.63	-0.20	-0.33
Al	138.00	2.20	2.45	2.23	-0.70	-0.48
Si	188.00	1.04	1.32	4.37	0.31	0.34
P	241.90	-0.06	0.49	6.62	1.92	1.92
S	239.00	1.51	1.12	6.97	-1.21	-1.29
Cl	299.10	-0.03	-0.28	10.07	0.80	0.69
CH ₄	296.34	-9.10	-7.53	11.06	0.47	1.61
NH ₃	235.69	-0.22	-2.12	22.75	-0.62	0.26
OH	300.92	5.20	2.40	22.17	1.40	2.24
OH ₂	292.65	-0.89	-2.99	26.60	0.99	1.77
FH	371.31	0.15	-2.37	28.46	3.15	3.77
SiH ₄	255.39	-7.20	-5.67	6.07	-1.10	-0.95
PH	234.11	1.93	2.54	4.99	1.08	1.10
PH ₂	226.37	3.39	3.95	3.72	0.13	0.15
PH ₃	227.82	-2.43	-3.18	13.77	0.86	0.75
SH	239.30	0.04	-0.31	11.96	1.64	1.52
HCl	294.46	-2.09	-2.19	14.43	3.09	2.95
C ₂ H ₂	264.58	-4.72	-5.85	27.06	-0.28	1.30
C ₂ H ₄	243.71	-5.03	-5.97	21.28	-2.02	-0.62
N ₂	359.37	-4.98	0.27	-55.67	-13.19	-14.67
O ₂	277.73	4.31	6.22	-22.40	-5.86	-6.26
P ₂	242.85	2.00	3.75	0.85	-0.91	-0.91
S ₂	215.74	1.26	3.37	-14.79	-9.42	-9.28
Cl ₂	265.08	-8.87	-6.25	-2.95	-4.61	-4.60
ClF	291.70	-7.41	-5.42	-8.38	-8.99	-8.96
ME		0.27	0.21	6.23	-0.99	-0.72
MAE		3.98	3.83	12.55	2.22	2.36
MARE		1.68	1.65	4.58	0.84	0.88

genISI2-hPC and genISI2-ePC, we found that on average they agree closely, both having MAE \approx 14 kcal/mol and MARE \approx 6 %, despite the fact that the results for individual molecules are different (for the molecules C₂H₂O₂, C₃H₄, and C₄H₈, they about 8-11 kcal/mol). Note that results in Table III differs from Tab. VI of Ref. [54] due to the different basis-set and different reference energy. For comparison with other popular functionals, see Table 2 of Ref. [78].

In Table IV we report the results for the ionization potential benchmark G21IP test [105], but CO and CS, which are spin-contaminated[78]. Tab. IV shows that genISI2-hPC and genISI2-ePC give similar results for all

systems, with differences less than 0.8 kcal/mol. Consequently, they have similar error statistics, with MAE \approx 2.3 kcal/mol and MARE \approx 0.8 %. These results are noticeably better than PBE15 (with MARE \approx 1.7 %) and GL2 (MARE \approx 4.6 %), as well as many other popular XC functionals [103, 104, 107]. Thus, the ePC strong-correlation functionals retain the accuracy of the hPC functional. For comparison with other popular functionals, see Table 2 of Ref. [78].

The largest error is found for the N_2 molecule. In the cation state we found a small energy-gap which gives a very large GL2 energy, so that the energy difference with respect to the neutral ground-state is reduced: genISI2 largely corrects the GL2 underestimation, but not completely.

V. CONCLUSIONS

We have constructed the enhanced point-and-charge (ePC) meta-GGA model for the strong-interaction functionals: $W_\infty[n]$, which represents the SCE limit of the adiabatic connection integrand $W_\infty[n] = \lim_{\alpha \rightarrow \infty} W_{xc,\alpha}[n]$ and $W'_\infty[n]$, which accounts for the electronic zero-point oscillations in the SCE limit. The ePC model resolves several shortcomings of the existing approximations, and fulfills important exact conditions: it is exact for the hydrogen atom, recovers the PC-GE2, satisfies important inequalities, in particular the non-negativity of $W'_\infty[n]$, and it is spin-dependent only for systems with few electrons and rapidly-varying densities. In particular, ePC is the first model that incorporates the full restoration of the PC-GE2, that should be relevant for Wigner crystals at low densities [20, 21].

In the case of systems with compact densities, as the atoms and molecules of Tables I,II,III and IV the ePC model performs somewhat better than the hPC state-of-the-art semilocal model.

For more diffuse densities, as the two-electron model density of Sec. IIIB and the s - and p -shells of hydrogenic orbitals presented in Sec. IIIC, the ePC and TPSS are remarkably accurate, while hPC and PC fail badly, even changing their signs. The density of these model systems resembles the one of systems described with pseudopotentials (i.e. with a vanishing density at the atomic core). Thus the ePC model can be expected to be very important in this case, and investigations in this direction are on the way.

The ePC model also has a remarkable performance for the quasi-2D IBM model system (see Sec. IIID), that represents a dimensional crossover from 3D UEG to 2D UEG where the density is still compact but with higher reduced gradients than in the case of atoms and molecules. As shown in Fig. 10, all the other strong-interaction models are failing badly. These facts show that the ePC model achieves a broader applicability compared with the existing strong-interaction semilocal models.

The ePC model can be further useful in the DFT development of XC functionals. Thus, its energy densities $w_\infty^{ePC}(\mathbf{r})$ and $w'_\infty^{ePC}(\mathbf{r})$, defined from $W_\infty^{ePC}[n] = \int d\mathbf{r} w_\infty^{ePC}(\mathbf{r})$ and $W'_\infty^{ePC}[n] = \int d\mathbf{r} w'_\infty^{ePC}(\mathbf{r})$, may be of interest for local interpolations along the adiabatic connection, a method for constructing XC functionals that has gained recent investigations and good progress [38–40, 42, 46, 47, 53, 108–111], being represented on the entire Jacob’s ladder [112], from the semilocal GGA and meta-GGA levels [47, 53] to the most sophisticated XC functionals, depending on the occupied and unoccupied KS orbitals and eigenvalues as well as the comotion functions $f_i(\mathbf{r})$ and the local normal modes $\omega_\mu(\mathbf{r})$ [46].

COMPUTATIONAL DETAILS

For the atomic and molecular calculations of Tables II, III and IV, and Figs. 13 and 14, we have used a modified version of the program package TURBOMOLE[113] together with the acmxc[114] script. The calculations have been performed within the resolution of identity (RI) approximation [115, 116] and the nearly complete 5ZaPaNR-CV all-electron basis sets[79], with the gridsize 4. We used self-consistent hybrid PBE15 orbitals, as discussed above, or the Localized Hartree-Fock orbitals [80, 81] for the atoms in Tab. II.

The SCE calculations of the atoms in Table I have been performed with the Engel code [117, 118], using accurate numerical OEP-EXX orbitals and densities, in a logarithmic grid. The calculations for Hooke’s atoms, two-electron exponential densities, quasi-2D IBM, perturbed UEG and the s - and p -hydrogenic shells use exact densities.

ACKNOWLEDGMENTS

F.D.S, E.F. and F.S. acknowledge the financial support from PRIN project no. 2022LM2K5X, Adiabatic Connection for Correlation in Crystals (AC^3). L.A.C. and F.D.S. acknowledge the financial support from ICSC - Centro Nazionale di Ricerca in High Performance Computing, Big Data and Quantum Computing, funded by European Union - NextGenerationEU - PNRR.

DATA AVAILABILITY

The data that support the findings of this article are not publicly available upon publication because it is not technically feasible and/or the cost of preparing, depositing, and hosting the data would be prohibitive within the terms of this research project. The data are available from the authors upon reasonable request.

-
- [1] P. Hohenberg and W. Kohn, Inhomogeneous electron gas, *Phys. Rev.* **136**, B864 (1964).
- [2] W. Kohn and L. J. Sham, Self-consistent equations including exchange and correlation effects, *Phys. Rev.* **140**, A1133 (1965).
- [3] K. Burke, Perspective on density functional theory, *J. Chem. Phys.* **136**, 150901 (2012).
- [4] P. J. Hasnip, K. Refson, M. I. J. Probert, J. R. Yates, S. J. Clark, and C. J. Pickard, Density functional theory in the solid state, *Philos. Trans. R. Soc. A* **372**, 20130270 (2014).
- [5] F. Giustino, *Materials Modelling Using Density Functional Theory: Properties and Predictions* (Oxford University Press, 2014).
- [6] A. D. Becke, Perspective: Fifty years of density-functional theory in chemical physics, *J. Chem. Phys.* **140**, 18A301 (2014).
- [7] R. O. Jones, Density functional theory: Its origins, rise to prominence, and future, *Rev. Mod. Phys.* **87**, 897 (2015).
- [8] W. Kohn, A. D. Becke, and R. G. Parr, Density functional theory of electronic structure, *J. Phys. Chem.* **100**, 12974 (1996).
- [9] W. Kohn, Nobel lecture: Electronic structure of matter-wave functions and density functionals, *Rev. Mod. Phys.* **71**, 1253 (1999).
- [10] G. E. Scuseria and V. N. Staroverov, Chapter 24 - progress in the development of exchange-correlation functionals, in *Theory and Applications of Computational Chemistry*, edited by C. E. Dykstra, G. Frenking, K. S. Kim, and G. E. Scuseria (Elsevier, Amsterdam, 2005) pp. 669–724.
- [11] D. C. Langreth and J. P. Perdew, The exchange-correlation energy of a metallic surface, *Solid State Comm.* **17**, 1425 (1975).
- [12] O. Gunnarsson and B. I. Lundqvist, Exchange and correlation in atoms, molecules, and solids by the spin-density-functional formalism, *Phys. Rev. B* **13**, 4274 (1976).
- [13] A. Savin, F. Colonna, and R. Pollet, Adiabatic connection approach to density functional theory of electronic systems, *Int. J. Quantum Chem.* **93**, 166 (2003).
- [14] A. J. Cohen, P. Mori-Sánchez, and W. Yang, Assessment and formal properties of exchange-correlation functionals constructed from the adiabatic connection, *J. Chem. Phys.* **127**, 034101 (2007).
- [15] M. Ernzerhof, Construction of the adiabatic connection, *Chem. Phys. Lett.* **263**, 499 (1996).
- [16] K. Burke, M. Ernzerhof, and J. P. Perdew, The adiabatic connection method: a non-empirical hybrid, *Chem. Phys. Lett.* **265**, 115 (1997).
- [17] F. Colonna and A. Savin, Correlation energies for some two- and four-electron systems along the adiabatic connection in density functional theory, *J. Chem. Phys.* **110**, 2828 (1999).
- [18] P. Gori-Giorgi, G. Vignale, and M. Seidl, Electronic zero-point oscillations in the strong-interaction limit of density functional theory, *J. Chem. Theory Comput.* **5**, 743 (2009).
- [19] M. Seidl, P. Gori-Giorgi, and A. Savin, Strictly correlated electrons in density-functional theory: A general formulation with applications to spherical densities, *Phys. Rev. A* **75**, 042511 (2007).
- [20] M. Seidl, J. P. Perdew, and S. Kurth, Density functionals for the strong-interaction limit, *Phys. Rev. A* **62**, 012502 (2000).
- [21] M. Seidl, J. P. Perdew, and S. Kurth, Erratum: Density functionals for the strong-interaction limit [*phys. rev. a* **62**, 012502 (2000)], *Phys. Rev. A* **72**, 029904 (2005).
- [22] M. Seidl, J. P. Perdew, and S. Kurth, Simulation of all-order density-functional perturbation theory, using the second order and the strong-correlation limit, *Phys. Rev. Lett.* **84**, 5070 (2000).
- [23] A. Görling and M. Levy, Correlation-energy functional and its high-density limit obtained from a coupling-constant perturbation expansion, *Phys. Rev. B* **47**, 13105 (1993).
- [24] S. Jana, S. Śmigaj, L. A. Constantin, and P. Samal, Generalizing double-hybrid density functionals: Impact of higher-order perturbation terms, *J. Chem. Theory Comput.* **16**, 7413 (2020).
- [25] Z.-F. Liu and K. Burke, Adiabatic connection in the low-density limit, *Phys. Rev. A* **79**, 064503 (2009).
- [26] A. Görling and M. Levy, Exact kohn-sham scheme based on perturbation theory, *Phys. Rev. A* **50**, 196 (1994).
- [27] A. Görling and M. Levy, Hardness of molecules and the band gap of solids within the kohn-sham formalism: A perturbation-scaling approach, *Phys. Rev. A* **52**, 4493 (1995).
- [28] P. Gori-Giorgi, M. Seidl, and G. Vignale, Density-functional theory for strongly interacting electrons, *Phys. Rev. Lett.* **103**, 166402 (2009).
- [29] F. Malet and P. Gori-Giorgi, Strong correlation in kohn-sham density functional theory, *Phys. Rev. Lett.* **109**, 246402 (2012).
- [30] G. Friesecke, A. Gerolin, and P. Gori-Giorgi, The strong-interaction limit of density functional theory, in *Density Functional Theory: Modeling, Mathematical Analysis, Computation*, edited by E. Cancès and G. Friesecke (Springer International Publishing, Cham, 2023) pp. 183–266.
- [31] M. Seidl, J. P. Perdew, and M. Levy, Strictly correlated electrons in density-functional theory, *Phys. Rev. A* **59**, 51 (1999).
- [32] J. P. Perdew, S. Kurth, and M. Seidl, Exploring the adiabatic connection between weak- and strong-interaction limits in density functional theory, *Int. J. Mod. Phys. B* **15**, 1672 (2001).
- [33] R. Magyar, W. Terilla, and K. Burke, Accurate adiabatic connection curve beyond the physical interaction strength, *J. Chem. Phys.* **119**, 696 (2003).
- [34] Z.-F. Liu and K. Burke, Adiabatic connection for strictly correlated electrons, *J. Chem. Phys.* **131**, 124124 (2009).
- [35] J. Sun, Extension to negative values of the coupling constant of adiabatic connection for interaction-strength interpolation, *J. Chem. Theory Comput.* **5**, 708 (2009).
- [36] M. Seidl and P. Gori-Giorgi, Adiabatic connection at negative coupling strengths, *Phys. Rev. A* **81**, 012508 (2010).

- [37] P. Gori-Giorgi and M. Seidl, Density functional theory for strongly-interacting electrons: perspectives for physics and chemistry, *Phys. Chem. Chem. Phys.* **12**, 14405 (2010).
- [38] A. Mirtschink, M. Seidl, and P. Gori-Giorgi, Energy densities in the strong-interaction limit of density functional theory, *J. Chem. Theory Comput.* **8**, 3097 (2012).
- [39] Y. Zhou, H. Bahmann, and M. Ernzerhof, Construction of exchange-correlation functionals through interpolation between the non-interacting and the strong-correlation limit, *J. Chem. Phys.* **143**, 124103 (2015).
- [40] S. Vuckovic, T. J. Irons, A. Savin, A. M. Teale, and P. Gori-Giorgi, Exchange-correlation functionals via local interpolation along the adiabatic connection, *J. Chem. Theory Comput.* **12**, 2598 (2016).
- [41] E. Fabiano, P. Gori-Giorgi, M. Seidl, and F. Della Sala, Interaction-strength interpolation method for main-group chemistry: benchmarking, limitations, and perspectives, *J. Chem. Theory Comput.* **12**, 4885 (2016).
- [42] S. Vuckovic, T. J. Irons, L. O. Wagner, A. M. Teale, and P. Gori-Giorgi, Interpolated energy densities, correlation indicators and lower bounds from approximations to the strong coupling limit of dft, *Phys. Chem. Chem. Phys.* **19**, 6169 (2017).
- [43] S. Vuckovic and P. Gori-Giorgi, Simple fully nonlocal density functionals for electronic repulsion energy, *J. Phys. Chem. Lett.* **8**, 2799 (2017).
- [44] S. Giarrusso, P. Gori-Giorgi, F. Della Sala, and E. Fabiano, Assessment of interaction-strength interpolation formulas for gold and silver clusters, *J. Chem. Phys.* **148**, 134106 (2018).
- [45] S. Vuckovic, P. Gori-Giorgi, F. Della Sala, and E. Fabiano, Restoring size consistency of approximate functionals constructed from the adiabatic connection, *J. Phys. Chem. Lett.* , 3137–3142 (2018).
- [46] D. P. Kooi and P. Gori-Giorgi, Local and global interpolations along the adiabatic connection of dft: a study at different correlation regimes, *Theor. Chem. Acc.* **137**, 166 (2018).
- [47] L. A. Constantin, Correlation energy functionals from adiabatic connection formalism, *Phys. Rev. B* **99**, 085117 (2019).
- [48] E. Fabiano, S. Śmiga, S. Giarrusso, T. J. Daas, F. Della Sala, I. Grabowski, and P. Gori-Giorgi, Investigation of the exchange-correlation potentials of functionals based on the adiabatic connection interpolation, *J. Chem. Theory Comput.* **15**, 1006 (2019).
- [49] S. Śmiga and L. A. Constantin, Modified interaction-strength interpolation method as an important step toward self-consistent calculations, *J. Chem. Theory Comput.* **16**, 4983 (2020).
- [50] S. Śmiga, F. Della Sala, P. Gori-Giorgi, and E. Fabiano, Self-consistent implementation of kohn-sham adiabatic connection models with improved treatment of the strong-interaction limit, *J. Chem. Theory Comput.* **18**, 5936 (2022).
- [51] S. Vuckovic, A. Gerolin, T. J. Daas, H. Bahmann, G. Friesecke, and P. Gori-Giorgi, Density functionals based on the mathematical structure of the strong-interaction limit of dft, *WIRE Comput. Mol. Sci.* **13**, e1634 (2023).
- [52] L. A. Constantin, S. Jana, S. Śmiga, and F. Della Sala, Adiabatic connection interaction strength interpolation method made accurate for the uniform electron gas, *J. Chem. Phys.* **159**, 244111 (2023).
- [53] S. Jana, S. Śmiga, L. A. Constantin, and P. Samal, Semilocal meta-gga exchange-correlation approximation from adiabatic connection formalism: Extent and limitations, *J. Phys. Chem. A* **127**, 8685 (2023).
- [54] L. A. Constantin, S. Śmiga, and F. Della Sala, Towards adiabatic-connection interpolation model with broader applicability, *Phys. Rev. B* **109**, 235129 (2024).
- [55] J. P. Perdew, K. Burke, and M. Ernzerhof, Generalized gradient approximation made simple, *Phys. Rev. Lett.* **77**, 3865 (1996).
- [56] J. P. Perdew, J. Tao, V. N. Staroverov, and G. E. Scuseria, Meta-generalized gradient approximation: Explanation of a realistic nonempirical density functional, *J. Chem. Phys.* **120**, 6898 (2004).
- [57] S. Azadi and N. D. Drummond, Low-density phase diagram of the three-dimensional electron gas, *Phys. Rev. B* **105**, 245135 (2022).
- [58] J. P. Perdew, A. Ruzsinszky, J. Sun, N. K. Nepal, and A. D. Kaplan, Interpretations of ground-state symmetry breaking and strong correlation in wavefunction and density functional theories, *Proc. Nat. Acad. Sci.* **118**, e2017850118 (2021).
- [59] A. Ruzsinszky, N. K. Nepal, J. M. Pitarke, and J. P. Perdew, Constraint-based wave vector and frequency dependent exchange-correlation kernel of the uniform electron gas, *Phys. Rev. B* **101**, 245135 (2020).
- [60] C. M. Horowitz, C. R. Proetto, and J. M. Pitarke, Universal exchange-correlation surface asymptotics: Metal slabs versus semi-infinite metal surfaces, *Phys. Rev. Lett.* **134**, 256401 (2025).
- [61] S.-K. Ma and K. A. Brueckner, Correlation energy of an electron gas with a slowly varying high density, *Phys. Rev.* **165**, 18 (1968).
- [62] C. D. Hu and D. C. Langreth, Beyond the random-phase approximation in nonlocal-density-functional theory, *Phys. Rev. B* **33**, 943 (1986).
- [63] J. Tao, J. P. Perdew, L. M. Almeida, C. Fiolhais, and S. Kümmel, Nonempirical density functionals investigated for jellium: Spin-polarized surfaces, spherical clusters, and bulk linear response, *Phys. Rev. B* **77**, 245107 (2008).
- [64] L. A. Constantin, F. Sarcinella, E. Fabiano, and F. Della Sala, Nonlocal exchange and correlation energy functionals using the yukawa potential as ingredient: Application to the linear response of the uniform electron gas, *Phys. Rev. B* **104**, 165114 (2021).
- [65] F. Della Sala, E. Fabiano, and L. A. Constantin, Kinetic-energy-density dependent semilocal exchange-correlation functionals, *Int. J. Quant. Chem.* **116**, 1641 (2016).
- [66] J. Sun, B. Xiao, and A. Ruzsinszky, Communication: Effect of the orbital-overlap dependence in the meta generalized gradient approximation, *The Journal of Chemical Physics* **137**, 051101 (2012).
- [67] K. J. Daas, D. P. Kooi, T. Benyahia, M. Seidl, and P. Gori-Giorgi, Large-z atoms in the strong-interaction limit of dft: Implications for gradient expansions and for the lieb-oxford bound, *J. Chem. Phys.* **159**, 234114 (2023).

- [68] J. Tao, J. P. Perdew, V. N. Staroverov, and G. E. Scuseria, Climbing the density functional ladder: Nonempirical meta-generalized gradient approximation designed for molecules and solids, *Phys. Rev. Lett.* **91**, 146401 (2003).
- [69] J. Tao and Y. Mo, Accurate semilocal density functional for condensed-matter physics and quantum chemistry, *Phys. Rev. Lett.* **117**, 073001 (2016).
- [70] J. W. Furness, N. Sengupta, J. Ning, A. Ruzsinszky, and J. Sun, Examining the order-of-limits problem and lattice constant performance of the tao-mo functional, *The Journal of Chemical Physics* **152**, 244112 (2020).
- [71] H. Francisco, A. C. Cancio, and S. B. Trickey, Reworking the tao-mo exchange-correlation functional. i. reconsideration and simplification, *The Journal of Chemical Physics* **159**, 214102 (2023).
- [72] A. Ruzsinszky, J. Sun, B. Xiao, and G. I. Csonka, A meta-gga made free of the order of limits anomaly, *Journal of Chemical Theory and Computation* **8**, 2078 (2012)
- [73] J. W. Furness and J. Sun, Enhancing the efficiency of density functionals with an improved iso-orbital indicator, *Phys. Rev. B* **99**, 041119 (2019).
- [74] J. Sun, B. Xiao, Y. Fang, R. Haunschild, P. Hao, A. Ruzsinszky, G. I. Csonka, G. E. Scuseria, and J. P. Perdew, Density functionals that recognize covalent, metallic, and weak bonds, *Phys. Rev. Lett.* **111**, 106401 (2013).
- [75] L. A. Constantin, E. Fabiano, and F. Della Sala, Hartree potential dependent exchange functional, *J. Chem. Phys.* **145**, 084110 (2016).
- [76] J. Tao, V. N. Staroverov, G. E. Scuseria, and J. P. Perdew, Exact-exchange energy density in the gauge of a semilocal density-functional approximation, *Phys. Rev. A* **77**, 012509 (2008).
- [77] E. H. Lieb and S. Oxford, Improved lower bound on the indirect coulomb energy, *International Journal of Quantum Chemistry* **19**, 427 (1981).
- [78] L. A. Constantin, E. Fabiano, and F. Della Sala, Nonempirical adiabatic connection correlation functional from hartree-fock orbitals, *J. Phys. Chem. Lett.* **16**, 3378 (2025).
- [79] D. S. Ranasinghe, M. J. Frisch, and G. A. Petersson, Core-core and core-valence correlation energy atomic and molecular benchmarks for li through ar, *J. Chem. Phys.* **143**, 214110 (2015).
- [80] F. Della Sala and A. Görling, Efficient localized Hartree-Fock methods as effective exact-exchange Kohn-Sham methods for molecules, *J. Chem. Phys.* **115**, 5718 (2001).
- [81] F. Della Sala and A. Görling, The asymptotic region of the Kohn-Sham exchange potential in molecules, *J. Chem. Phys.* **116**, 5374 (2002).
- [82] M. Seidl, Strong-interaction limit of density-functional theory, *Phys. Rev. A* **60**, 4387 (1999).
- [83] L. A. Constantin, E. Fabiano, and F. Della Sala, Kinetic and exchange energy densities near the nucleus, *Computation* **4**, 19 (2016).
- [84] F. Della Sala, E. Fabiano, and L. A. Constantin, Kohn-sham kinetic energy density in the nuclear and asymptotic regions: Deviations from the von weizsäcker behavior and applications to density functionals, *Phys. Rev. B* **91**, 035126 (2015).
- [85] L. Pollack and J. Perdew, Evaluating density functional performance for the quasi-two-dimensional electron gas, *J. Phys. : Condens. Matter* **12**, 1239 (2000).
- [86] S. Karimi and C. A. Ullrich, Three-to two-dimensional crossover in time-dependent density-functional theory, *Phys. Rev. B* **90**, 245304 (2014).
- [87] L. A. Constantin, Simple effective interaction for dimensional crossover, *Phys. Rev. B* **93**, 121104 (2016).
- [88] A. D. Kaplan, K. Wagle, and J. P. Perdew, Collapse of the electron gas from three to two dimensions in kohn-sham density functional theory, *Phys. Rev. B* **98**, 085147 (2018).
- [89] C. Horowitz, C. Proetto, and J. Pitarke, Construction of a semilocal exchange density functional from a three-dimensional electron gas collapsing to two dimensions, *Phys. Rev. B* **108**, 115119 (2023).
- [90] A. Ghosh, S. Jana, M. Hossain, D. Rani, S. Śmiga, and P. Samal, Advancing excited-state properties of two-dimensional materials using a dielectric-dependent hybrid functional, *Phys. Rev. B* **112**, 045128 (2025).
- [91] A. Ghosh, S. Jana, T. Rauch, F. Tran, M. A. L. Marques, S. Botti, L. A. Constantin, M. K. Niranjan, and P. Samal, Efficient and improved prediction of the band offsets at semiconductor heterojunctions from meta-gga density functionals: A benchmark study, *J. Chem. Phys.* **157**, 124108 (2022).
- [92] W. Jones and W. H. Young, Density functional theory and the von weizsacker method, *J. Phys. C: Solid State Phys.* **4**, 1322 (1971).
- [93] M. Weimer, F. Della Sala, and A. Görling, Multi-configuration optimized effective potential method for a density-functional treatment of static correlation, *J. Chem. Phys.* **128**, 144109 (2008).
- [94] I. Y. Zhang and X. Xu, On the top rung of jacob's ladder of density functional theory: Toward resolving the dilemma of sie and nce, *WIREs Comp. Mol. Sci.* **11**, e1490 (2021).
- [95] A. J. Cohen, P. Mori-Sánchez, and W. Yang, Fractional spins and static correlation error in density functional theory, *J. Chem. Phys.* **129**, 121104 (2008).
- [96] P. Mori-Sánchez, A. J. Cohen, and W. Yang, Discontinuous nature of the exchange-correlation functional in strongly correlated systems, *Phys. Rev. Lett.* **102**, 066403 (2009).
- [97] A. J. Cohen, P. Mori-Sánchez, and W. Yang, Second-order perturbation theory with fractional charges and fractional spins, *J. Chem. Theory Comput.* **5**, 786 (2009).
- [98] B. G. Janesko, E. Proynov, J. Kong, G. Scalmani, and M. J. Frisch, Practical density functionals beyond the overdelocalization-underbinding zero-sum game, *J. Phys. Chem. Lett.* **8**, 4314 (2017).
- [99] J. Kirkpatrick, B. McMorro, D. H. P. Turban, A. L. Gaunt, J. S. Spencer, A. G. D. G. Matthews, A. Obika, L. ouis Thiry, M. Fortunato, D. Pfau, L. R. Castellanos, S. Petersen, A. W. R. Nelson, P. Kohli, P. Mori-Sánchez, D. Hassabis, and A. J. Cohen, Pushing the frontiers of density functionals by solving the fractional electron problem, *Science* **374**, 1385-1389 (2021).
- [100] R. van Leeuwen and E. J. Baerends, Exchange-correlation potential with correct asymptotic behavior, *Phys. Rev. A* **49**, 2421 (1994).
- [101] C. Adamo and V. Barone, Toward reliable density functional methods without adjustable parameters: The PBE0 model, *J. Chem. Phys.* **110**, 6158 (1999).

- [102] R. Haunschuld and W. Klopper, Theoretical reference values for the ae6 and bh6 test sets from explicitly correlated coupled-cluster theory, *Theor. Chem. Acc.* **131**, 1112 (2012).
- [103] L. Goerigk and S. Grimme, A general database for main group thermochemistry, kinetics, and non-covalent interactions - assessment of common and reparameterized (meta-) gga density functionals, *J. Chem. Theory Comput.* **6**, 107 (2010).
- [104] L. Goerigk and S. Grimme, A thorough benchmark of density functional methods for general main group thermochemistry, kinetics, and noncovalent interactions, *Phys. Chem. Chem. Phys.* **13**, 6670 (2011).
- [105] L. A. Curtiss, K. Raghavachari, G. W. Trucks, and J. A. Pople, Gaussian-2 theory for molecular energies of first- and second-row compounds, *J. Chem. Phys.* **94**, 7221 (1991).
- [106] B. J. Lynch and D. G. Truhlar, Small representative benchmarks for thermochemical calculations, *J. Phys. Chem. A* **107**, 8996 (2003).
- [107] E. Fabiano, L. A. Constantin, P. Cortona, and F. Della Sala, Global hybrids from the semiclassical atom theory satisfying the local density linear response, *J. Chem. Theory Comput.* **11**, 122 (2015).
- [108] H. Bahmann, Y. Zhou, and M. Ernzerhof, The shell model for the exchange-correlation hole in the strong-correlation limit, *J. Chem. Phys.* **145**, 124104 (2016).
- [109] S. Vuckovic, M. Levy, and P. Gori-Giorgi, Augmented potential, energy densities, and virial relations in the weak- and strong-interaction limits of dft, *J. Chem. Phys.* **147**, 214107 (2017).
- [110] S. Giarrusso and P. Gori-Giorgi, Exchange-correlation energy densities and response potentials: Connection between two definitions and analytical model for the strong-coupling limit of a stretched bond, *J. Phys. Chem. A* **124**, 2473 (2020).
- [111] S. Giarrusso and P. Gori-Giorgi, Correction to “exchange–correlation energy densities and response potentials: Connection between two definitions and analytical model for the strong-coupling limit of a stretched bond”, *J. Phys. Chem. A* **124**, 9895 (2020).
- [112] J. P. Perdew and K. Schmidt, Jacob’s ladder of density functional approximations for the exchange–correlation energy, *AIP Conf. Proc.* **577**, 1 (2001).
- [113] Y. J. Franzke, C. Holzer, J. H. Andersen, T. Begušić, F. Bruder, S. Coriani, F. Della Sala, E. Fabiano, D. A. Fedotov, S. Fürst, S. Gillhuber, R. Grotjahn, M. Kaupp, M. Kehry, M. Krstić, F. Mack, S. Majumdar, B. D. Nguyen, S. M. Parker, F. Pauly, A. Pausch, E. Perlt, G. S. Phun, A. Rajabi, D. Rappoport, B. Samal, T. Schrader, M. Sharma, E. Tapavicza, R. S. Treß, V. Voora, A. Wodyński, J. M. Yu, B. Zerulla, F. Furche, C. Hättig, M. Sierka, D. P. Tew, and F. Weigend, Turbomole: Today and tomorrow, *J. Chem. Theory Comput.* **19**, 6859 (2023).
- [114] E. Fabiano, <https://github.com/e-fabiano/acmxc> (2024), accessed: 2024-11-25.
- [115] C. Hättig and F. Weigend, Cc2 excitation energy calculations on large molecules using the resolution of the identity approximation, *J. Chem. Phys.* **113**, 5154 (2000).
- [116] C. Hättig, A. Hellweg, and A. Köhn, Distributed memory parallel implementation of energies and gradients for second-order møller–plesset perturbation theory with the resolution-of-the-identity approximation, *Phys. Chem. Chem. Phys.* **8**, 1159 (2006).
- [117] E. Engel and S. H. Vosko, Accurate optimized-potential-model solutions for spherical spin-polarized atoms: Evidence for limitations of the exchange-only local spin-density and generalized-gradient approximations, *Phys. Rev. A* **47**, 2800 (1993).
- [118] E. Engel, Orbital-dependent functionals for the exchange–correlation energy: A third generation of density functionals, in *A Primer in Density Functional Theory*, edited by C. Fiolhais, F. Nogueira, and M. A. L. Marques (Springer Berlin Heidelberg, Berlin, Heidelberg, 2003) pp. 56–122.